One-loop contributions in the effective field theory for the $\Lambda N \to NN$ transition

A. Pérez-Obiol,[1,*] D. R. Entem,[2,†] B. Juliá-Díaz,[1,3,‡] and A. Parreño[1,§]

[1]*Departament d'Estructura i Constituents de la Matèria, Institut de Ciències del Cosmos (ICC), Universitat de Barcelona, Martí Franquès 1, E-08028 Barcelona, Spain*

[2]*Grupo de Física Nuclear and IUFFyM, Universidad de Salamanca, E-37008 Salamanca, Spain*

[3]*ICFO-Institut de Ciències Fotòniques, Avenida Carl Friedrich Gauss 3, E-08860 Castelldefels (Barcelona), Spain*

(Received 21 March 2013; published 29 April 2013)

We consider the $\Lambda N \to NN$ weak transition, responsible for a large fraction of the nonmesonic weak decay of hypernuclei. We follow the previously derived effective field theory and compute the next-to-leading one-loop corrections. Explicit expressions for all diagrams are provided, which result in contributions to all relevant partial waves.

DOI: 10.1103/PhysRevC.87.044614 PACS number(s): 13.75.Ev, 21.80.+a, 25.80.Pw, 13.30.Eg

I. INTRODUCTION

One of the major challenges in nuclear physics is to understand the interactions among hadrons from first principles. For more than 20 years, many research groups have directed their efforts to develop effective field theories (EFTs), working with the idea of separating the nuclear force in long-range and short-range components. The underlying premise was that low-energy processes, as the ones encountered in nuclear physics, should not be affected by the specific details of the high-energy physics.

The typical energies associated with nuclear phenomena suggest that the appropriate degrees of freedom are nucleons and pions (or the ground-state baryon and pseudoscalar octets for processes involving strangeness), interacting derivatively as it is dictated by the effective chiral Lagrangian. The nuclear interaction is characterized by the presence of very different scales, going from the values of the masses of the light pseudoscalar bosons to the ones of the ground-state octet baryons. The EFT formalism makes use of this separation of scales to construct an expansion of the Lagrangian in terms of a parameter built up from ratios of these scales. For example, in the study of the low-energy nucleon-nucleon interaction, a clear separation of scales is seen between the external momentum of the interacting nucleons, a soft scale which typically takes values up to the pion mass, and a hard scale corresponding to the nucleon mass. While the long-range part of this interaction is governed by the light scale through the pion-exchange mechanism, short-range forces are accounted for by zero-range contact operators, organized according to an increasing number of derivatives. These contact terms, which respect chiral symmetry, have values which are not constrained by the chiral Lagrangian, and therefore, their relative strength (encapsulated in the size of the low-energy coefficients, LECs) has to be obtained from a fit to nuclear observables. The large amount of experimental data for the interaction among pions and nucleons has made it possible to perform successful EFT calculations of the strong nucleon-nucleon interaction up to fourth order in the momentum expansion [$\mathcal{O}(p^4)$], at next-to-next-to-next-to-leading order ($\mathrm{N^3LO}$) in the heavy-baryon formalism [1,2]. In the weak sector, the study of nucleon-nucleon parity violation (PV) with an EFT at leading order has been undertaken in Ref. [3], where the authors discuss existing and possible few-body measurements that can help in constraining the relevant (five) low-energy constants at order p in the momentum expansion and the ones associated with dynamical pions.

In the strange sector, the experimental situation is less favorable owing to the short lifetime of hyperons, unstable against the weak interaction. This fact complicates the extraction of information regarding the strong interaction among baryons in free space away from the nucleonic sector. Nevertheless, SU(3) extensions of the EFT for nucleons and pions have been developed at leading order (LO) [4–7] and next-to-leading (NLO) order [8]. In the present work we consider the weak four-body $\Lambda N \to NN$ interaction, which is accessible experimentally by looking at the decay of Λ-hypernuclei, bound systems composed of nucleons and one Λ hyperon. These aggregates decay weakly through mesonic ($\Lambda \to N\pi$) and nonmesonic ($\Lambda N \to NN$) modes, the former being suppressed for mass numbers of the order or larger than 5, owing to the Pauli blocking effect acting on the outgoing nucleon. In contrast to the weak NN PV interaction, which is masked by the much stronger parity conserving (PC) strong NN signal, the weak $|\Delta S| = 1$ ΛN interaction has the advantage of presenting a change of flavor as a signature, favoring its detection in the presence of the strong interaction.

The first studies of the weak ΛN interaction using a lowest order effective theory were presented in Refs. [9–11]. These works included the exchange of the lighter pseudoscalar mesons while parametrizing the short-range part of the interaction with contact terms at order $\mathcal{O}(q^0)$, where q denotes the momentum exchanged between the interacting baryons. While the results of Ref. [11] show that it is possible to reproduce the hypernuclear decay data with the lowest order effective Lagrangian, the stability of the momentum expansion has to be checked by including the next order in the EFT. If an EFT can be built for the weak $\Lambda N \to NN$ transition,

*axel@ecm.ub.edu
†entem@usal.es
‡bruno@ecm.ub.edu
§assum@ecm.ub.edu

the values for the LECs of the theory, which encode the high-energy components of the interaction, should vary within a reasonable and natural range when one includes higher orders in the calculation. Compared to the LO calculation, which involves two LECs, the unknown baryon-baryon-kaon vertices and the pseudoscalar cutoff parameter in the form factor, the NLO calculation introduces additional unknowns, namely, the parameters associated with the new contact terms (three when one neglects the small value of the momentum of the initial particles, a nucleon and a hyperon bound in the hypernucleus, in front of the momentum of the two outgoing nucleons) and the couplings appearing in the two-pion exchange diagrams. Therefore, to constrain the EFT at NLO, one needs to collect enough data, either through the accurate measure of hypernuclear decay observables or through the measure of the inverse reaction in free space, $np \to \Lambda p$. Unfortunately, the small values of the cross sections for the weak strangeness production mechanism, of the order of 10^{-12} mb [12–14], has prevented, for the time being, its consideration as part of the experimental data set, despite the effort invested in extracting different polarization observables for this process [15,16]. At present, quantitative experimental information on the $|\Delta S| = 1$ weak interaction in the baryonic sector comes from the measure of the total and partial decay rates of hypernuclei and an asymmetry in the number of protons detected parallel and antiparallel to the polarization axis, which comes from the interference between the PC and PV weak amplitudes. Because observables from one hypernucleus to another can be related through hypernuclear structure coefficients, one has to be careful in selecting the data that can be used in the EFT calculation. For example, while one may indeed expect measurements from different p-shell hypernuclei, say, $A = 12$ and 16, to provide with the same constraint, the situation is different when including data from s-shell hypernuclei like $A = 5$. For the latter, the initial ΛN pair can only be in a relative s state, while for the former, relative p states are allowed as well.

In this paper we present the analytic expressions to be included at NLO in the effective theory for the weak ΛN interaction. These expressions have been derived by considering four-fermion contact terms with a derivative operator insertion together with the two-pion exchange mechanism.

The paper is organized as follows. In Sec. II we introduce the Lagrangians and the power counting scheme we use to calculate the relevant Feynman diagrams. In Secs. III and IV we present the LO and NLO potentials for the $\Lambda N \to NN$ transition, and a comparison between both contributions is performed in Sec. V. We conclude and summarize in Sec. VI.

II. INTERACTION LAGRANGIANS AND COUNTING SCHEME

The nonmesonic weak decay of the Λ involves both the strong and the electroweak interactions. The Λ decay is mediated by the presence of a nucleon which in the simplest meson-exchange picture, exchanges a meson, e.g., π, K, with the Λ. Thus, computing the transition requires the knowledge of the strong and weak Lagrangians involving all the hadrons

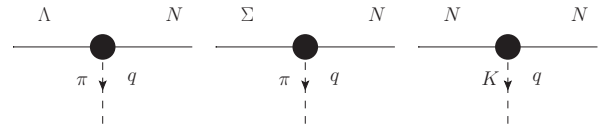

FIG. 1. Weak vertices for the $\Lambda N\pi$, $\Sigma N\pi$, and NNK stemming from the Lagrangians in Eq. (2.1). The weak vertex is represented by a solid black circle.

entering in the process. In this section we describe the strong and weak Lagrangians entering at LO and NLO in the $\Lambda N \to NN$ interaction.

The weak interaction between the Σ, Λ, and N baryons and the pseudoscalar π and K mesons is described by the phenomenological Lagrangians

$$\begin{aligned}
\mathcal{L}^{w}_{\Lambda N\pi} &= -iG_F m_\pi^2 \overline{\Psi}_N (A + B\gamma^5)\vec{\tau}\cdot\vec{\pi}\,\Psi_\Lambda, \\
\mathcal{L}^{w}_{\Sigma N\pi} &= -iG_F m_\pi^2 \overline{\Psi}_N (\vec{A}_{\Sigma_i} + \vec{B}_{\Sigma_i}\gamma^5)\cdot\vec{\pi}\,\Psi_{\Sigma_i}, \\
\mathcal{L}^{w}_{NNK} &= -iG_F m_\pi^2 \left[\overline{\psi}_N \begin{pmatrix}0\\1\end{pmatrix} (C_K^{\rm PV} + C_K^{\rm PC}\gamma_5)\,(\phi^K)^\dagger \psi_N \right. \\
&\quad \left. + \overline{\psi}_N \psi_N\,(D_K^{\rm PV} + D_K^{\rm PC}\gamma_5)\,(\phi^K)^\dagger \begin{pmatrix}0\\1\end{pmatrix}\right],
\end{aligned} \tag{2.1}$$

where $G_F m_\pi^2 = 2.21 \times 10^{-7}$ is the weak Fermi coupling constant, γ are the Dirac matrices, and τ the Pauli matrices (see Fig. 1). The index i appearing in the Σ field refers to the different isospurion states for the Σ hyperon:

$$\Psi_{\Sigma\frac{1}{2}} = \begin{pmatrix} -\sqrt{\frac{2}{3}}\Sigma_+ \\ \frac{1}{\sqrt{3}}\Sigma_0 \end{pmatrix}, \quad \Psi_{\Sigma\frac{3}{2}} = \begin{pmatrix} 0 \\ -\frac{1}{\sqrt{3}}\Sigma_+ \\ \sqrt{\frac{2}{3}}\Sigma_0 \\ \Sigma_- \end{pmatrix}. \tag{2.2}$$

The PV and PC structures, $\vec{A}_{\Sigma_i}$ and $\vec{B}_{\Sigma_i}$, contain the corresponding weak coupling constants together with the isospin operators τ^a for $\frac{1}{2} \to \frac{1}{2}$ transitions and T^a for $\frac{1}{2} \to \frac{3}{2}$ transitions. The weak couplings $A = 1.05$, $B = -7.15$, $A_{\Sigma\frac{1}{2}} = -0.59$, $A_{\Sigma\frac{3}{2}} = 2.00$, $B_{\Sigma\frac{1}{2}} = -15.68$, and $B_{\Sigma\frac{3}{2}} = -0.26$ [17] are fixed to reproduce the experimental data of the corresponding hyperon decays, while the ones involving kaons, $C_K^{\rm PC} = -18.9$, $D_K^{\rm PC} = 6.63$, $C_K^{\rm PV} = 0.76$, and $D_K^{\rm PV} = 2.09$, are derived using SU(3) symmetry.

The other two weak vertices entering at the considered order (Fig. 2) are obtained from the weak SU(3) chiral Lagrangian,

$$\begin{aligned}
\mathcal{L}^{w}_{\Lambda N\pi\pi} &= G_F m_\pi^2 \frac{h_{2\pi}}{f_\pi^2}(\vec{\pi}\cdot\vec{\pi})\overline{\Psi}\Psi_\Lambda, \\
\mathcal{L}^{w}_{\Lambda N} &= iG_F m_\pi^2 h_{\Lambda N}\overline{\Psi}\Psi_\Lambda,
\end{aligned} \tag{2.3}$$

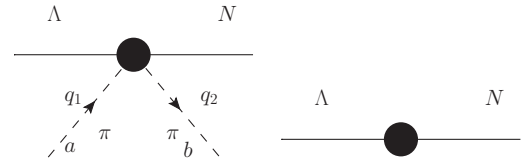

FIG. 2. Weak vertices corresponding to the $\Lambda N\pi\pi$ and ΛN interactions. The corresponding Lagrangians are given in Eq. (2.3).

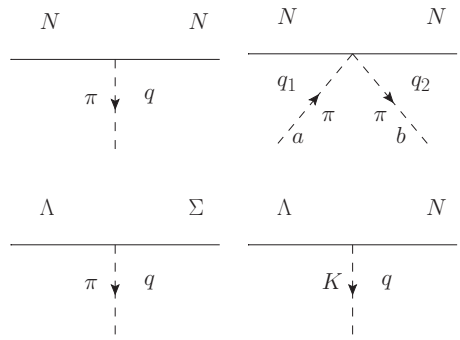

FIG. 3. Strong vertices for the $NN\pi$, $NN\pi\pi$, $\Lambda\Sigma\pi$, and ΛNK which arise from the Lagrangians in Eq. (2.4).

with $h_{2\pi} = (D+3F)/(8\sqrt{6}G_F m_\pi^2) = -10.13$ MeV and $h_{\Lambda N} = -(D+3F)/(\sqrt{6}G_F m_\pi^2) = 81.02$ MeV. D and F are the couplings parametrizing the weak chiral SU(3) Lagrangian, and can be fitted through the pole model to the experimentally known hyperon decays. In that case, one finds that when s-wave amplitudes are correctly reproduced, p-wave amplitude predictions disagree with the experiment [18].

The strong vertices for the interaction between our baryonic and mesonic degrees of freedom are obtained from the strong SU(3) chiral Lagrangian [18],

$$\begin{aligned}
\mathcal{L}^s_{NN\pi} &= -\frac{g_A}{2f_\pi}\overline{\Psi}\gamma^\mu\gamma_5\vec{\tau}\Psi\cdot\partial_\mu\vec{\pi},\\
\mathcal{L}^s_{NN\pi\pi} &= -\frac{1}{4f_\pi^2}\overline{\Psi}\gamma^\mu\vec{\tau}\cdot(\vec{\pi}\times\partial_\mu\vec{\pi})\Psi,\\
\mathcal{L}^s_{\Lambda\Sigma\pi} &= -\frac{D_s}{\sqrt{3}}\overline{\Psi}_\Lambda\gamma^\mu\gamma_5\Psi_\Sigma\cdot\partial_\mu\vec{\pi},\\
\mathcal{L}^s_{\Lambda NK} &= \frac{D_s+3F_s}{2\sqrt{3}f_\pi}\overline{\Psi}_N\gamma^\mu\gamma_5\,\partial_\mu\phi_K\Psi_\Lambda,
\end{aligned} \tag{2.4}$$

where we have taken the convention which gives us $\Psi_\Sigma\cdot\vec{\pi} = \Psi_{\Sigma_+}\pi_- + \Psi_{\Sigma_-}\pi_+ + \Psi_{\Sigma_0}\pi_0$, and we consider $g_A = 1.290$, $f_\pi = 92.4$ MeV, $D_s = 0.822$, and $F_s = 0.468$. These strong coupling constants are taken from NN interaction models such as the Jülich [19] or Nijmegen [20] potentials. The four interaction vertices corresponding to these Lagrangians are depicted in Fig. 3.

Once the interaction Lagrangians involving the relevant degrees of freedom have been presented, we need to define the power counting scheme which allows us to organize the different contributions to the full amplitude.

A. Power counting scheme

The amplitude for the $\Lambda N \to NN$ transition is built as the sum of medium- and long-range one-meson exchanges (i.e., π and K), the contribution from the two-pion exchanges, and the contribution of the contact interactions up to $\mathcal{O}(q^2/M^2)$, as described below. The order in which the different terms enter the perturbative expansion of the amplitudes is given by the so-called Weinberg power counting scheme [21].

In our calculations we employ the heavy-baryon formalism [22]. This technique introduces a perturbative expansion in the baryon masses appearing in the Lagrangians, so that this new large scale does not disrupt the well-defined Weinberg power counting. It is worth noting that, in the heavy-baryon formalism, terms of the type $\overline{\Psi}_B\gamma^5\Psi_B$ are subleading in front of terms like $\overline{\Psi}_B\Psi_B$, because they show up at one order higher in the heavy-baryon expansion. In our calculation, we choose to keep both terms in our Lagrangians of Eqs. (2.1) because the experimental values for the couplings B_Λ and B_Σ are much larger than A_Λ and A_Σ. For example, $A_\Lambda = 1.05$ and $B_\Lambda = -7.15$ [18].

Our calculation is characterized by the presence of different octet baryons in the relevant Feynman diagrams, contributing in both the spinors and the propagators. The spinors for the incoming Λ and N with masses M_Λ and M_N, energies E_p^Λ and E_p^N, and momenta $\vec{p}$ and $-\vec{p}$ are

$$\begin{aligned}
u_1\big(E_p^\Lambda,\vec{p}\big) &= \sqrt{\frac{E_p^\Lambda+M_\Lambda}{2M_\Lambda}}\begin{pmatrix}1\\ \frac{\vec{\sigma}_1\cdot\vec{p}}{E_p^\Lambda+M_\Lambda}\end{pmatrix},\\
u_2\big(E_p^N,-\vec{p}\big) &= \sqrt{\frac{E_p^N+M_N}{2M_N}}\begin{pmatrix}1\\ -\frac{\vec{\sigma}_2\cdot\vec{p}}{E_p^N+M_N}\end{pmatrix},
\end{aligned} \tag{2.5}$$

and for the outgoing nucleons with momenta $\vec{p}\,'$ and $-\vec{p}\,'$, and energy $E' \equiv \frac{1}{2}(E_p^\Lambda + E_p^N)$,

$$\begin{aligned}
\bar{u}_1(E',\vec{p}\,') &= \sqrt{\frac{E'+M_N}{2M_N}}\left(1-\frac{\vec{\sigma}_1\cdot\vec{p}\,'}{E'+M_N}\right),\\
\bar{u}_2(E',-\vec{p}\,') &= \sqrt{\frac{E'+M_N}{2M_N}}\left(1+\frac{\vec{\sigma}_2\cdot\vec{p}\,'}{E'+M_N}\right).
\end{aligned} \tag{2.6}$$

The relativistic propagator of a baryon with mass M_B and momentum p reads

$$\frac{i}{\not{p}-M_B+i\epsilon} = \frac{i(\not{p}+M_B)}{p^2-M_B^2+i\epsilon}. \tag{2.7}$$

Heavy-baryon expanding with these spinors and propagators introduces mass differences $(M_\Lambda - M_N,\ M_\Sigma - M_\Lambda)$ in the baryonic propagators. A reasonable approach would be to consider these mass differences of order $\mathcal{O}(\vec{q}^{\,2}/\Lambda^2)$, $M_B = \overline{M} + \mathcal{O}(\vec{q}^{\,2}/\Lambda^2)$, and thus they would not enter in the loop diagrams. We have chosen to leave the physical masses in both the initial and the final spinors and also in the intermediate propagators; i.e., we consider the mass differences as another scale in the heavy-baryon expansion. The corresponding SU(3) symmetric limit is also given at the end of Sec. IV B and can be easily obtained from our expressions by setting the mass differences, which we explicitly retain, to zero.

The procedure we follow to compute the different Feynman diagrams entering the transition amplitude is the following: First we write down the relativistic expressions for each diagram, and then afterwards we perform the heavy-baryon expansion.

In the next sections we describe the LO and NLO contributions to the process $\Lambda N \to NN$, following the scheme presented here. The explicit expressions and details of the calculations are given in the Appendices.

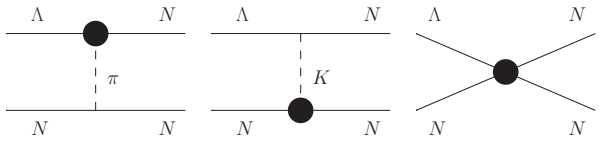

FIG. 4. LO contributions to the EFT coming from one-pion-exchange, one-kaon-exchange and contact interactions.

III. LEADING ORDER CONTRIBUTIONS

For completeness, we rewrite here the LO EFT already presented in Ref. [11] and then build the NLO contributions in the next section.

At tree level, the transition potential $\Lambda N \to NN$ involves the LO contact terms and π and K exchanges, as depicted in Fig. 4. First, the contact interaction can be written as the most general Lorentz invariant potential with no derivatives. The four-fermion (4P) interaction in momentum space at LO (in units of G_F) is

$$V_{4P}(\vec{q}\,) = C_0^0 + C_0^1\ \vec{\sigma}_1\vec{\sigma}_2, \tag{3.1}$$

where C_0^0 and C_0^1 are low-energy constants which need to be fitted by direct comparison to experimental data. In Ref. [11] we presented several sets of values which were to a large extent compatible with the scarce data on hypernuclear decay.

The potentials for the one-pion and one-kaon exchanges, as functions of transferred momentum $\vec{q} \equiv \vec{p}\,' - \vec{p}$, read, respectively [23],

$$V_\pi(\vec{q}\,) = -\frac{G_F m_\pi^2 g_{NN\pi}}{2M_N}\left(A_\pi - \frac{B_\pi}{2\overline{M}}\vec{\sigma}_1\,\vec{q}\right) \times \frac{\vec{\sigma}_2\,\vec{q}}{-q_0^2 + \vec{q}^{\,2} + m_\pi^2}\vec{\tau}_1\cdot\vec{\tau}_2, \tag{3.2}$$

$$V_K(\vec{q}\,) = \frac{G_F m_\pi^2 g_{\Lambda NK}}{2\overline{M}}\left(\hat{A} + \frac{\hat{B}}{2M_N}\vec{\sigma}_2\,\vec{q}\right) \times \frac{\vec{\sigma}_1\,\vec{q}}{-q_0^2 + \vec{q}^{\,2} + m_K^2}, \tag{3.3}$$

where $m_\pi = 138$ MeV and $m_K = 495$ MeV, $q_0 \equiv \frac{1}{2}(M_\Lambda - M_N)$, $g_{NN\pi} \equiv \frac{g_A M_N}{f_\pi}$, $g_{\Lambda NK} \equiv -\frac{D_s+3F_s}{2\sqrt{3}f_\pi}$, $\overline{M} \equiv \frac{1}{2}(M_N + M_\Lambda)$, and

$$\hat{A} = \left(\frac{C_K^{\rm PV}}{2} + D_K^{\rm PV} + \frac{C_K^{\rm PV}}{2}\vec{\tau}_1\vec{\tau}_2\right),$$
$$\hat{B} = \left(\frac{C_K^{\rm PC}}{2} + D_K^{\rm PC} + \frac{C_K^{\rm PC}}{2}\vec{\tau}_1\vec{\tau}_2\right).$$

IV. NEXT-TO-LEADING ORDER CONTRIBUTIONS

The NLO contribution to the weak decay process, $\Lambda N \to NN$, includes contact interactions with one and two derivative operators, caramel diagrams, and two-pion-exchange diagrams.

TABLE I. All possible PC and PV NLO operational structures connecting the initial and final spin and angular momentum states. There are a total of 20.

Order	Parity	Structures
0	PC	$1, \vec{\sigma}_1\cdot\vec{\sigma}_2$
1	PV	$\vec{\sigma}_1\cdot\vec{q}, \vec{\sigma}_1\cdot\vec{p}, \vec{\sigma}_2\cdot\vec{q}, \vec{\sigma}_2\cdot\vec{p}, (\vec{\sigma}_1\times\vec{\sigma}_2)\cdot\vec{q}, (\vec{\sigma}_1\times\vec{\sigma}_2)\cdot\vec{p},$
2	PC	$\vec{q}^{\,2}, \vec{p}^{\,2}, (\vec{\sigma}_1\cdot\vec{\sigma}_2)\vec{q}^{\,2}, (\vec{\sigma}_1\cdot\vec{\sigma}_2)\vec{p}^{\,2}, (\vec{\sigma}_1\cdot\vec{q})(\vec{\sigma}_2\cdot\vec{q}), (\vec{\sigma}_1\cdot\vec{p})(\vec{\sigma}_2\cdot\vec{p}), (\vec{\sigma}_1+\vec{\sigma}_2)\cdot(\vec{q}\times\vec{p})$
2	PV	$\vec{q}\cdot\vec{p}, (\vec{\sigma}_1\cdot\vec{\sigma}_2)\vec{q}\cdot\vec{p}, (\vec{\sigma}_1\cdot\vec{q})(\vec{\sigma}_2\cdot\vec{p}), (\vec{\sigma}_1\cdot\vec{p})(\vec{\sigma}_2\cdot\vec{q}), (\vec{\sigma}_1-\vec{\sigma}_2)\cdot(\vec{q}\times\vec{p})$

A. NLO contact potential

In principle, the NLO contact potential should include, in the center of mass, structures involving both the initial ($\vec{p}$) and final ($\vec{p}\,'$) momenta, or independent linear combinations, e.g., $\vec{q} \equiv \vec{p}\,' - \vec{p}$ and $\vec{p}$. Table I lists all these possible structures. At NLO there are 18 LECs—6 PV ones at order $\mathcal{O}(q/M)$, 7 PC ones at order $\mathcal{O}(q^2/M^2)$, and 5 PV ones at order $\mathcal{O}(q^2/M^2)$—which must be fitted to experiment. This is not feasible with current experimental data on hypernuclear decay. A reasonable way to reduce the number of LECs and render the fitting procedure more tractable is to note that the pionless weak decay mechanism we are interested in takes place inside a bound hypernucleus. Thus, one can consider that in the $\Lambda N \to NN$ transition potential the initial baryons have a fairly small momentum. Moreover, the final nucleons gain an extra momentum from the surplus mass of the Λ ($M_\Lambda - M_N = 116$ MeV), which in most cases make it possible to consider $\vec{p}\,' \gg \vec{p}$. In this case, one may approximate $\vec{q} \simeq \vec{p}\,'$ and $\vec{p} = 0$. Within this approximation, the NLO part of the contact potential reads (in units of G_F)

$$V_{4P}(\vec{q}\,) = C_1^0\,\frac{\vec{\sigma}_1\vec{q}}{2M_N} + C_1^1\,\frac{\vec{\sigma}_2\vec{q}}{2M_N} + \mathrm{i}\,C_1^2\,\frac{(\vec{\sigma}_1\times\vec{\sigma}_2)\,\vec{q}}{2M_N} + C_2^0\,\frac{\vec{\sigma}_1\vec{q}\;\vec{\sigma}_2\vec{q}}{4M_N^2} + C_2^1\,\frac{\vec{\sigma}_1\vec{\sigma}_2\,\vec{q}^{\,2}}{4M_N^2} + C_2^2\,\frac{\vec{q}^{\,2}}{4M_N^2}. \tag{4.1}$$

Using strong and weak LO contact interactions and two baryonic propagators, one can also build three diagrams that enter at NLO. These caramel-like diagrams are shown in Fig. 5. They differ only in the position of the strong and weak vertices and in the mass of the upper-leg baryonic propagator. To write a general expression for the three caramel diagrams we label the mass of the upper-leg propagating baryon M_α ($M_a = M_N$, $M_b = M_\Lambda$, and $M_c = M_\Sigma$) and the corresponding

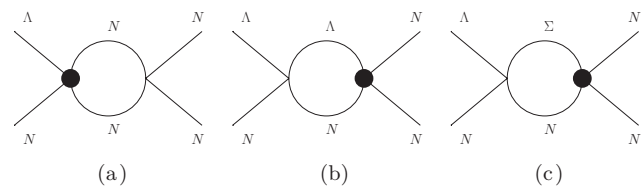

FIG. 5. Caramel diagrams contributing to the process at NLO.

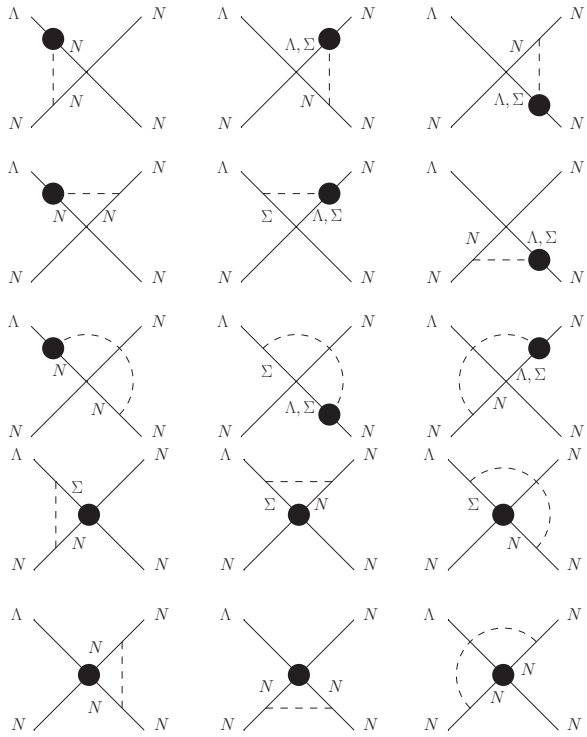

FIG. 6. Corrections to the LO contact interactions. The contributions of all these diagrams can be accounted for by an adequate shift of the coefficients of the LO contact terms.

strong and weak contact vertices $C^{\alpha}_{S(s)} + C^{\alpha}_{T(s)}\vec{\sigma}_1\cdot\vec{\sigma}_2$ and $C^{\alpha}_{S(w)} + C^{\alpha}_{T(w)}\vec{\sigma}_1\cdot\vec{\sigma}_2$, where $\alpha = a, b, c$ corresponds to the labels of Fig. 5. It is also convenient to define $M_\alpha = M_N + \Delta_\alpha$. In the heavy-baryon formalism these diagrams only contribute with an imaginary part of the form

$$V_\alpha = i\frac{G_F m_\pi^2}{16\pi M_N}\left(C^{\alpha}_{S(s)} + C^{\alpha}_{T(s)}\vec{\sigma}_1\cdot\vec{\sigma}_2\right)\left(C^{\alpha}_{S(w)} + C^{\alpha}_{T(w)}\vec{\sigma}_1\cdot\vec{\sigma}_2\right) \times\sqrt{(\Delta_b-\Delta_\alpha)\left[\tfrac{1}{2}(\Delta_b+\Delta_\alpha)+M_N\right]+\vec{p}^{\,2}}. \tag{4.2}$$

Few more details are given in Appendix A.

One pion corrections to the LO contact interactions, shown in Fig. 6, also enter at NLO. The net contribution of these diagrams is to shift the coefficients of the LO contact terms with functions dependent on m_π, $M_\Lambda - M_N$, and $M_\Sigma - M_N$.

B. Two-pion-exchange diagrams

The two-pion-exchange contributions are organized according to the different topologies—balls, triangles, and boxes—such that most of the integration techniques are shared by each class of diagrams. There are two types of ball diagrams, of which only one gives a nonzero contribution, depicted in Fig. 7. In addition, there are four triangle diagrams, shown in Fig. 8, and two box and crossed-box diagrams, shown in Fig. 9. The topologies contain, respectively, zero, one, and two baryonic propagators, which may correspond to N or Σ baryons. All the diagrams contain two relativistic propagators from the $2-\pi$ exchange.

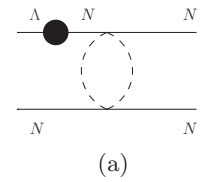

FIG. 7. The ball diagram contributing to the process at NLO.

The technical details of the evaluation of the Feynman diagrams for the ball, triangle, and box diagrams are given in Appendices B, C, and D, respectively. The main technique used is to introduce a number of master integrals, which appear in different diagrams, and which reduce the mathematical complexity of the problem (see Appendix E). Once they are defined, we derive a number of relations between the master integrals, which can in most cases be easily checked. Full details are provided to ensure the future use of these expressions.

Using the labels defined in Figs. 7, 8 and 9 we organize the contributions of all the $2-\pi$ exchange diagrams in Eq. (4.3). The corresponding coefficients in terms of the coupling constants, baryon and meson masses, and momenta can be read off from the full expressions given in the Appendices B, C, and D:

$$\begin{aligned}
V_a &= c_{a1}\,\vec{\tau}_1\cdot\vec{\tau}_2, \quad V_b = c_{b1}, \quad V_c = c_{c1}\,\vec{\tau}_1\cdot\vec{\tau}_2,\\
V_d &= [c_{d1} + c_{d2}\,\vec{\sigma}_1\cdot\vec{q} + c_{d3}\,(\vec{q}\cdot\vec{p})\\
&\quad + c_{d4}\,\vec{\sigma}_1\cdot(\vec{q}\times\vec{p})](\vec{\tau}_1\cdot\vec{\tau}_2),\\
V_e &= (c_{e1} + c_{e2}\vec{\sigma}_1\cdot\vec{q})(\vec{\tau}_1\cdot\vec{\tau}_2),
\end{aligned} \tag{4.3}$$

$$\begin{aligned}
V_f &= [c_{f1} + c_{f2}\vec{\sigma}_1\cdot\vec{\sigma}_2 + c_{f3}\vec{\sigma}_1\cdot\vec{q} + c_{f4}(\vec{\sigma}_1\times\vec{\sigma}_2)\cdot\vec{q}\\
&\quad + c_{f5}(\vec{\sigma}_1\cdot\vec{q})(\vec{\sigma}_2\cdot\vec{q}) + c_{f6}(\vec{\sigma}_1\cdot\vec{q})(\vec{\sigma}_2\cdot\vec{p})\\
&\quad + c_{f7}\vec{\sigma}_1\cdot(\vec{p}\times\vec{q}) + c_{f8}\vec{\sigma}_2\cdot(\vec{p}\times\vec{q})](c'_{f1} + c'_{f2}\,\vec{\tau}_1\cdot\vec{\tau}_2),\\
V_g &= [c_{g1} + c_{g2}\vec{\sigma}_1\cdot\vec{\sigma}_2 + c_{g3}(\vec{\sigma}_1\cdot\vec{q})(\vec{\sigma}_2\cdot\vec{q})]\\
&\quad\times(c'_{g1} + c'_{g2}\,\vec{\tau}_1\cdot\vec{\tau}_2)\\
&\quad + [c_{g4}\vec{\sigma}_1\cdot\vec{q} + c_{g5}(\vec{\sigma}_1\times\vec{\sigma}_2)\cdot\vec{q}](c''_{g1} + c''_{g2}\,\vec{\tau}_1\cdot\vec{\tau}_2),\\
V_h &= [c_{h1} + c_{h2}\vec{\sigma}_1\cdot\vec{\sigma}_2 + c_{h3}\vec{\sigma}_1\cdot\vec{q} + c_{h4}(\vec{\sigma}_1\times\vec{\sigma}_2)\cdot\vec{q}\\
&\quad + c_{h5}(\vec{\sigma}_1\cdot\vec{q})(\vec{\sigma}_2\cdot\vec{q}) + c_{h6}(\vec{\sigma}_1\cdot\vec{q})(\vec{\sigma}_2\cdot\vec{p})\\
&\quad + c_{h7}\vec{\sigma}_1\cdot(\vec{p}\times\vec{q}) + c_{h8}\vec{\sigma}_2\cdot(\vec{p}\times\vec{q})](c'_{h1} + c'_{h2}\,\vec{\tau}_1\cdot\vec{\tau}_2),\\
V_i &= [c_{i1} + c_{i2}\vec{\sigma}_1\cdot\vec{\sigma}_2 + c_{i3}(\vec{\sigma}_1\cdot\vec{q})(\vec{\sigma}_2\cdot\vec{q})]\\
&\quad\times(c'_{i1} + c'_{i2}\,\vec{\tau}_1\cdot\vec{\tau}_2)\\
&\quad + [c_{i4}\vec{\sigma}_1\cdot\vec{q} + c_{i5}(\vec{\sigma}_1\times\vec{\sigma}_2)\cdot\vec{q}](c''_{i1} + c''_{i2}\,\vec{\tau}_1\cdot\vec{\tau}_2).
\end{aligned} \tag{4.4}$$

Considering the SU(3) limit where all the baryon masses are considered to take the same value ($q_0 = q'_0 = 0$) the

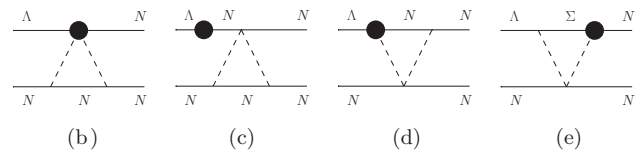

FIG. 8. Triangle diagrams which contribute to the process at NLO.

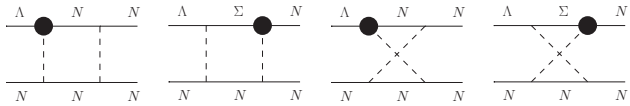

FIG. 9. Box diagrams which contribute to the process at NLO.

expressions above become much more simple. Defining

$$At(q) \equiv \frac{1}{2q}\arctan\left(\frac{q}{2m_\pi}\right),$$
$$L(q) \equiv \frac{\sqrt{4m_\pi^2+q^2}}{q}\ln\left(\frac{\sqrt{4m_\pi^2+q^2}+q}{2m_\pi}\right),$$
$$q \equiv \sqrt{\vec{q}^{\,2}},$$

and extracting the baryonic poles and the polynomial terms, one obtains

$$V_a = -\frac{h_{\Lambda N}}{192\pi^2 f_\pi^4 (M_\Lambda - M_N)}\left(4m_\pi^2+q^2\right)L(q)(\vec{\tau}_1\cdot\vec{\tau}_2), \quad (4.5)$$

$$V_b = \frac{3g_A^2 h_{2\pi}}{32\pi f_\pi^4}\left(2m_\pi^2+q^2\right)\,At\,(q), \quad (4.6)$$

$$V_c = -\frac{g_A^2 h_{\Lambda N}}{384\pi^2 f_\pi^4 (M_\Lambda - M_N)}\left(8m_\pi^2+5q^2\right)L(q)(\vec{\tau}_1\cdot\vec{\tau}_2), \quad (4.7)$$

$$V_d = \frac{g_A}{64\pi^2 f_\pi^3 M_N}L(q)(\vec{\tau}_1\cdot\vec{\tau}_2)\big[-2Bm_\pi^2 - B\vec{q}^{\,2} + B(\vec{q}\cdot\vec{p}) + 6AM_N(\vec{\sigma}_1\cdot\vec{q}) - 3iB\vec{\sigma}_1\cdot(\vec{q}\times\vec{p})\big], \quad (4.8)$$

$$V_e = \frac{\sqrt{3}D_s}{384\pi^2 f_\pi^3 M_N}L(q)\big[B_{\Sigma 1}\left(4m_\pi^2+3\vec{q}^{\,2}\right) - 4A_{\Sigma 1}M_N(\vec{\sigma}_1\cdot\vec{q})\big], \quad (4.9)$$

$$V_f = \frac{g_A^3}{512\pi^2 f_\pi^3 M_N\left(4m_\pi^2+\vec{q}^{\,2}\right)}L(q)(-3+2\vec{\tau}_1\cdot\vec{\tau}_2) \times\Big\{\frac{1}{6}B\big[448m_\pi^4+4m_\pi^2(-24\vec{q}\cdot\vec{p}+47\vec{q}^{\,2})+25\vec{q}^{\,4} - 36\vec{q}^{\,2}(\vec{q}\cdot\vec{p})\big]+4iB(4m_\pi^2+\vec{q}^{\,2})\vec{\sigma}_2\cdot(\vec{q}\times\vec{p}) - 4AM_N\left(8m_\pi^2+3\vec{q}^{\,2}\right)\vec{\sigma}_1\cdot\vec{q} + 2iB\left(8m_\pi^2+3\vec{q}^{\,2}\right)\vec{\sigma}_1\cdot(\vec{q}\times\vec{p}) + 4B\left(4m_\pi^2+\vec{q}^{\,2}\right)(\vec{\sigma}_1\cdot\vec{q})(\vec{\sigma}_2\cdot\vec{p}) - 4B\left(4m_\pi^2+\vec{q}^{\,2}\right)(\vec{\sigma}_1\cdot\vec{q})(\vec{\sigma}_2\cdot\vec{q}) - 4B\left(4m_\pi^2+\vec{q}^{\,2}\right)(\vec{q}\cdot\vec{p}-\vec{q}^{\,2})(\vec{\sigma}_1\cdot\vec{\sigma}_2) - 8iAM_N\left(4m_\pi^2+\vec{q}^{\,2}\right)(\vec{\sigma}_1\times\vec{\sigma}_2)\cdot\vec{q}\Big\}, \quad (4.10)$$

$$V_g = \frac{D_s g_A^2}{256\sqrt{3}\pi^2 f_\pi^3 M_N\left(4m_\pi^2+\vec{q}^{\,2}\right)}L(q) \times\Big[-\frac{1}{6}B_{\Sigma 2}\left(448m_\pi^4+188m_\pi^2\vec{q}^{\,2}+25\vec{q}^{\,4}\right) + 4A_{\Sigma 2}M_N\left(8m_\pi^2+3\vec{q}^{\,2}\right)(\vec{\sigma}_1\cdot\vec{q}) + 4B_{\Sigma 2}\left(4m_\pi^2+\vec{q}^{\,2}\right)(\vec{\sigma}_1\cdot\vec{q})(\vec{\sigma}_2\cdot\vec{q}) - 4B_{\Sigma 2}\left(4m_\pi^2+\vec{q}^{\,2}\right)\vec{q}^{\,2}(\vec{\sigma}_1\cdot\vec{\sigma}_2) - 8iA_{\Sigma 2}M_N\left(4m_\pi^2+\vec{q}^{\,2}\right)(\vec{\sigma}_1\times\vec{\sigma}_2)\cdot\vec{q}\Big], \quad (4.11)$$

$$V_h = \frac{g_A^3}{512\pi^2 f_\pi^3 M_N\left(4m_\pi^2+\vec{q}^{\,2}\right)}L(q)(3+2\vec{\tau}_1\cdot\vec{\tau}_2) \times\Big\{\frac{1}{6}B\big[448m_\pi^4+4m_\pi^2(-24\vec{q}\cdot\vec{p}+47\vec{q}^{\,2})+25\vec{q}^{\,4} - 36\vec{q}^{\,2}(\vec{q}\cdot\vec{p})\big]-4iB\left(4m_\pi^2+\vec{q}^{\,2}\right)\vec{\sigma}_2\cdot(\vec{q}\times\vec{p}) - 4AM_N\left(8m_\pi^2+3\vec{q}^{\,2}\right)\vec{\sigma}_1\cdot\vec{q} - 2iB\left(8m_\pi^2+3\vec{q}^{\,2}\right)\vec{\sigma}_1\cdot(\vec{q}\times\vec{p}) + 4B\left(4m_\pi^2+\vec{q}^{\,2}\right)(\vec{\sigma}_1\cdot\vec{q})(\vec{\sigma}_2\cdot\vec{p}) - 4B\left(4m_\pi^2+\vec{q}^{\,2}\right)(\vec{\sigma}_1\cdot\vec{q})(\vec{\sigma}_2\cdot\vec{q}) - 4B\left(4m_\pi^2+\vec{q}^{\,2}\right)(\vec{q}\cdot\vec{p}-\vec{q}^{\,2})(\vec{\sigma}_1\cdot\vec{\sigma}_2) + 8iAM_N\left(4m_\pi^2+\vec{q}^{\,2}\right)(\vec{\sigma}_1\times\vec{\sigma}_2)\cdot\vec{q}\Big\}, \quad (4.12)$$

$$V_i = \frac{D_s g_A^2}{256\sqrt{3}\pi^2 f_\pi^3 M_N\left(4m_\pi^2+\vec{q}^{\,2}\right)}L(q) \times\Big[\frac{1}{6}B_{\Sigma 3}\left(448m_\pi^4+188m_\pi^2\vec{q}^{\,2}+25\vec{q}^{\,4}\right) + A_{\Sigma 3}M_N\left(8m_\pi^2+3\vec{q}^{\,2}\right)(\vec{\sigma}_1\cdot\vec{q}) + 4B_{\Sigma 3}\left(4m_\pi^2+\vec{q}^{\,2}\right)(\vec{\sigma}_1\cdot\vec{q})(\vec{\sigma}_2\cdot\vec{q}) - 4B_{\Sigma 3}\left(4m_\pi^2+\vec{q}^{\,2}\right)\vec{q}^{\,2}(\vec{\sigma}_1\cdot\vec{\sigma}_2) + 4iA_{\Sigma 3}M_N\left(4m_\pi^2+\vec{q}^{\,2}\right)(\vec{\sigma}_1\times\vec{\sigma}_2)\cdot\vec{q}\Big]. \quad (4.13)$$

The isospin part for the potentials that contain Σ propagators (V_e, V_g, V_i) is taken into account by making the replacements:

$$A_{\Sigma 1} \to \tfrac{2}{3}\left(\sqrt{3}A_{\Sigma\frac{1}{2}} + A_{\Sigma\frac{3}{2}}\right)\vec{\tau}_1\cdot\vec{\tau}_2,$$
$$B_{\Sigma 1} \to \tfrac{2}{3}\left(\sqrt{3}B_{\Sigma\frac{1}{2}} + B_{\Sigma\frac{3}{2}}\right)\vec{\tau}_1\cdot\vec{\tau}_2,$$
$$A_{\Sigma 2} \to -\sqrt{3}A_{\Sigma\frac{1}{2}} + 2A_{\Sigma\frac{3}{2}} + \tfrac{2}{3}\left(\sqrt{3}A_{\Sigma\frac{1}{2}} + A_{\Sigma\frac{3}{2}}\right)\vec{\tau}_1\cdot\vec{\tau}_2,$$
$$B_{\Sigma 2} \to -\sqrt{3}B_{\Sigma\frac{1}{2}} + 2B_{\Sigma\frac{3}{2}} + \tfrac{2}{3}\left(\sqrt{3}B_{\Sigma\frac{1}{2}} + B_{\Sigma\frac{3}{2}}\right)\vec{\tau}_1\cdot\vec{\tau}_2,$$
$$A_{\Sigma 3} \to -\sqrt{3}A_{\Sigma\frac{1}{2}} + 2A_{\Sigma\frac{3}{2}} - \tfrac{2}{3}\left(\sqrt{3}A_{\Sigma\frac{1}{2}} + 2A_{\Sigma\frac{3}{2}}\right)\vec{\tau}_1\cdot\vec{\tau}_2,$$
$$B_{\Sigma 3} \to -\sqrt{3}B_{\Sigma\frac{1}{2}} + 2B_{\Sigma\frac{3}{2}} - \tfrac{2}{3}\left(\sqrt{3}B_{\Sigma\frac{1}{2}} + 2B_{\Sigma\frac{3}{2}}\right)\vec{\tau}_1\cdot\vec{\tau}_2.$$

Note that Eqs. (4.5) and (4.7) only have physical meaning away from the SU(3) limit.

We note here that the role played by the two-pion exchange mechanism in the weak decay of hypernuclei was also considered in Ref. [24]. This work scales the expressions obtained in the strong *NN* sector within the chiral unitary approach [25] to account for the PC amplitudes in the weak transitions, the scaling factor being the ratio between the weak and strong baryon-baryon-meson coupling constants.

Although the formalism is not directly comparable with our EFT approach, it provides an insight on the role played by the interferences between the different diagrams considered (one-meson exchange and uncorrelated and correlated two-pion exchanges).

V. BRIEF COMPARISON OF LO AND NLO CONTRIBUTIONS

In Eqs. (4.3) and (4.4) we provide the explicit momentum and spin structures arising from the different Feynman diagrams. Some features can be easily read off from the different terms. First, the ball in Fig. 7(a) and first two triangle diagrams in Figs. 8(b) and 8(c) only contribute to the PC part of the transition potential. Most other diagrams have a nontrivial contribution, involving all allowed momenta and spin structures.

To provide a sample of the contribution of the different diagrams to the full amplitude, we consider one particular transition, ${}^3S_1 \to {}^3S_1$. In particular, we compare the π and K exchanges with the ball, triangle, and box diagrams for the $\Lambda n \to nn$ interaction. Because the transition is PC, none of the parity-violating structures of Table I contribute. For structures of the type $(\vec{\sigma}_1 \cdot \vec{q})(\vec{\sigma}_2 \cdot \vec{q})$ we have that

$$(\vec{\sigma}_1 \cdot \vec{q})(\vec{\sigma}_2 \cdot \vec{q}) = \frac{\vec{q}^{\,2}}{3}(\vec{\sigma}_1 \cdot \vec{\sigma}_2) + \frac{\vec{q}^{\,2}}{3}\hat{S}_{12}(\hat{q}), \qquad (5.1)$$

where the tensor operator $\hat{S}_{12}(\hat{q})$ changes two units of angular momentum and does not contribute to this transition. The potential, therefore, depends only on the modulus of the momentum (or $\vec{q}^{\,2}$). To obtain the potential in position space we Fourier-transform the expressions for the one-meson-exchange contributions, Eqs. (3.2) and (3.3), and the loop expressions in the Appendices B, C, and D. More explicitly,

$$\tilde{V}(r) = \mathcal{F}[V(\vec{q}^{\,2})F(\vec{q}^{\,2})] \equiv \int_{-\infty}^{\infty} \frac{d^3q}{(2\pi)^3} e^{i\vec{q}\cdot\vec{r}} V(\vec{q}^{\,2})F(\vec{q}^{\,2}),$$

with $q \equiv |\vec{q}|$ and $r \equiv |\vec{r}|$ and where we have included a form factor to regularize the potential. Following the formalism developed in Ref. [23] we use a monopole form factor for the meson exchange contribution at each vertex, while the $2-\pi$ terms use a Gaussian form of the type $F(\vec{q}^{\,2}) \equiv e^{-\vec{q}^{\,4}/\Lambda^4}$.

The expressions for each loop have been calculated using dimensional regularization and are shown in Appendices B, C, and D. They are written in terms of the couplings appearing in Sec. II and of the master integrals appearing in Appendix E. η is the regularization parameter that appears when integrating in $D \equiv 4 - \eta$ dimensions. The modified minimal subtraction scheme ($\overline{MS}$) has been used; we have expanded in powers of η the expressions for the different loop contributions and then subtracted the term $R \equiv -\frac{2}{\eta} + \gamma - 1 - \ln(4\pi)$.

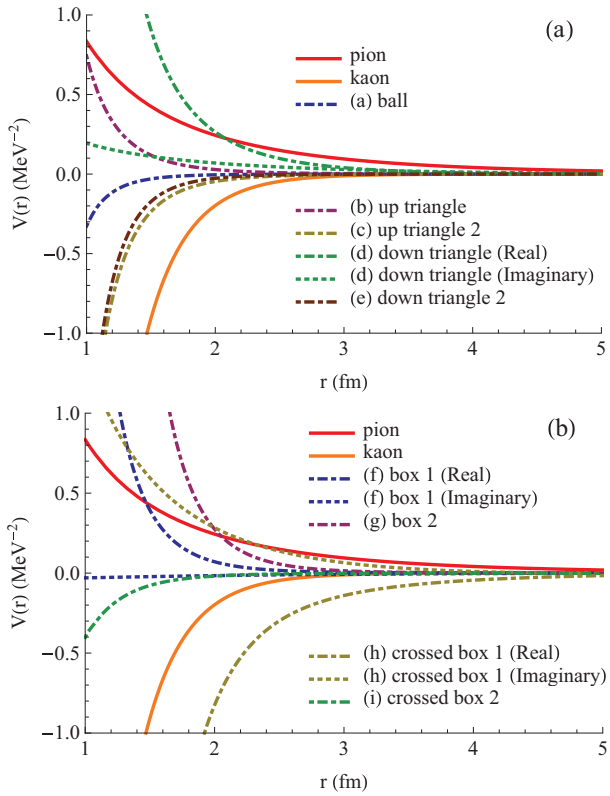

FIG. 10. (Color online) (a) Medium- to long-range part of the potentials for the one-pion-exchange, one-kaon-exchange, ball diagrams, and triangle diagrams. (b) Medium- to long-range part of the potentials for the one-pion-exchange, one-kaon-exchange, box, and crossed-box diagrams.

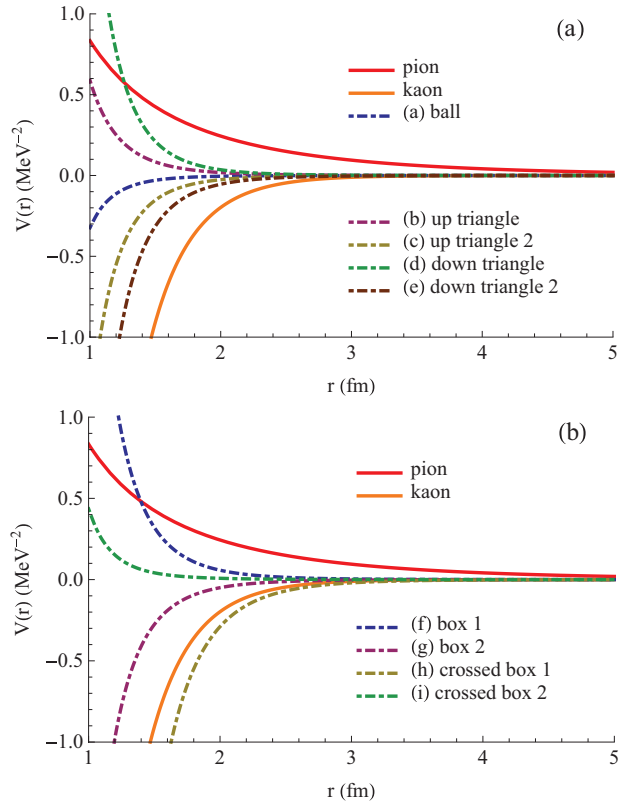

FIG. 11. (Color online) (a) Medium- to long-range part of the potentials in the SU(3) limit for the one-pion-exchange, one-kaon-exchange, ball diagrams, and triangle diagrams. (b) Medium- to long-range part of the potentials in the SU(3) limit for the one-pion-exchange, one-kaon-exchange, box, and crossed-box diagrams.

In Fig. 10, we show the respective contributions to the potential in position space. The contribution from the different $2-\pi$ exchange potentials are seen to be sizable at all distances. In particular, the box (f),(g),(h) and triangle (d) diagrams give larger contributions than the pion in the medium and long range. The ball diagram (a) and the triangles (c),(e),(h),(i) are attractive while all the others are repulsive. Notice that diagrams (d),(f),(h) contribute with an imaginary part. This is characteristic of diagrams with a $\Lambda N\pi$ vertex, which may be on shell because $M_\Lambda > M_N + m_\pi$. This imaginary part is taking into account the amplitude for the possible $\Lambda N \to NN\pi$ transition. We stress that the imaginary part of the box diagram (f) that comes from the baryonic pole has been extracted, so no iterated part is considered in Fig. 10.

Figure 11 shows the same potentials but taking $q_0 = q_0' = 0$. All diagrams seem to have a smaller contribution when the baryon mass differences are neglected. The attractive and repulsive character of the different potentials does not change except for the second box diagram and the second crossed-box diagram, which become attractive and repulsive, respectively, when taking the SU(3) limit.

VI. CONCLUSIONS

The weak decay of hypernuclei is dominated for large enough number of nucleons by the nonmesonic weak decay modes. In these modes, the bound Λ particle decays in the presence of nucleons by means of a process which involves weak and strong interaction vertices describing the production and absorption of mesons. The relevant, experimentally known, partial and total decay rates of hypernuclei are successfully described by meson-exchange models and also by a lowest-order EFT description of the weak $\Lambda N \to NN$ process, when appropriate nuclear wave functions are used for the initial and final nuclear systems. Nevertheless, the stability of the EFT approach which has to be tested by looking at higher orders in the theory, could not be analyzed yet, mainly because of the very scarce world database for such observables, a situation that should be improved in the near future.

In this article we have presented the one-loop contribution to the previously obtained LO EFT for the weak $\Delta S = 1$ ΛN transition.

As expected, the structure of the transition amplitude is considerably more involved than the corresponding LO amplitude and contains more LECs which ought to be fitted to data. In the present formal work we have solely presented the calculation of the amplitude terms and have not attempted to make any comparison to experimental data; therefore, no fit to extract the new unknowns has been performed. The different structures which appear in the obtained transition amplitude, involving spin, isospin, and orbital degrees of freedom, produce sizable contributions to all relevant partial waves. To illustrate this fact, we have presented the potential in r space corresponding to the different Feynman diagrams for the $^3S_1$-$^3S_1$ partial wave. Box and cross-box diagrams are found to produce substantial contributions at distances of the order of 1 fm, larger than the ones corresponding to the one-pion-exchange and one-kaon-exchange mechanisms. In view of this result, it would be interesting to see if one-loop contributions play an equivalent role in other partial wave transitions, testing possible cancellations or enhancements that would leave the results for the decay rates either unchanged or modified. A complete analysis of the higher order terms would require a larger set of independent hypernuclear decay measurements and a more accurate measure of some observables, especially those related to the parity violating asymmetry for s-shell and p-shell hypernuclei. Moreover, it would be desirable to arrange for alternative experiments focused to obtain information on the weak $\Delta S = 1$ interaction. A step in this direction was taken more than 10 years ago by experimental groups at Research Center for Nuclear Physics in Osaka (Japan) [15,16], by looking at the weak strangeness production reaction $np \to \Lambda p$. Unfortunately, the small value for the cross-section for this process precluded the compilation of new data. We think that it is important to foster new experimental avenues of approaching the weak interaction among baryons in the strange sector, and even try to recover the Osaka experiment within the research plan of the new experimental facilities devoted to the study of strange systems.

To ease the use of the obtained EFT amplitudes, we have provided the explicit analytic expressions for all diagrams which will in future work be implemented in the calculation of hypernuclear decay observables.

ACKNOWLEDGMENTS

We thank J. Soto, J. Tarrús, J. Haidenbauer, and A. Nogga for helpful comments and discussions. This work is partly supported by Grants No. FPA2010-21750-C02-02, No. FIS2008-00784 TOQATA, and No. FIS2011-24154 from MICINN, No. 283286 from European Community-Research Infrastructure Integrating Activity "Study of Strongly Interacting Matter," No. CSD2007-00042 from Spanish Ingenio-Consolider 2010 Program CPAN, and No. 2009SGR-1289 from Generalitat de Catalunya. A.P-O. acknowledges support by the APIF Ph.D. program of the University of Barcelona. B.J.D. is supported by the Ramon y Cajal program.

APPENDIX A: CARAMEL DIAGRAMS

Using the same notation that is described in Sec. IV A we write a general expression for the three caramel diagrams that depends on the label $\alpha = a, b, c$, which corresponds, respectively, to the masses and vertices of Figs. 12, 13, and 14.

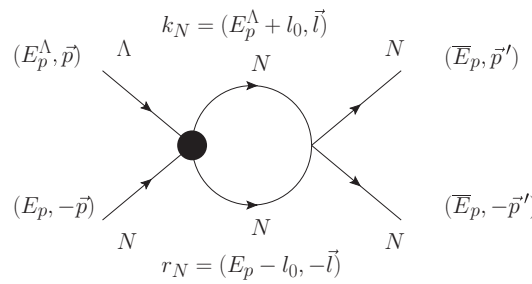

FIG. 12. First caramel-type Feynman diagram.

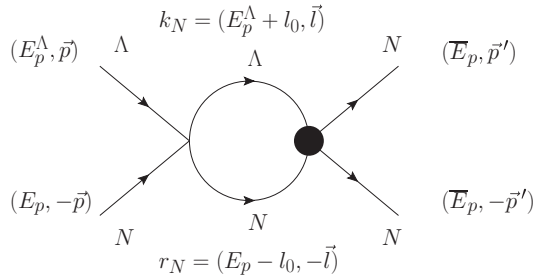

FIG. 13. Second caramel-type Feynman diagram.

The relativistic expression for our caramel diagrams is

$$V_\alpha = iG_F m_\pi^2 \left(C^\alpha_{S(s)} + C^\alpha_{T(s)} \vec{\sigma}_1 \cdot \vec{\sigma}_2\right)\left(C^\alpha_{S(w)} + C^\alpha_{T(w)} \vec{\sigma}_1 \cdot \vec{\sigma}_2\right) \times \int \frac{d^4 l}{(2\pi)^4} \frac{1}{(E_p - l_0)^2 - \vec{l}^2 - M_N^2 + i\epsilon} \times \frac{1}{\left(E_p^\Lambda + l_0\right)^2 - \vec{l}^2 - M_\alpha^2}.$$

To not miss the relativistic pole we must first integrate the temporal part (l_0) before heavy-baryon expanding the expression. Proceeding in this manner one obtains a purely imaginary part (the real is suppressed in the heavy-baryon expansion):

$$V_\alpha = -\frac{G_F m_\pi^2}{4M_N}\left(C^\alpha_{S(s)} + C^\alpha_{T(s)} \vec{\sigma}_1 \cdot \vec{\sigma}_2\right)\left(C^\alpha_{S(w)} + C^\alpha_{T(w)} \vec{\sigma}_1 \cdot \vec{\sigma}_2\right) \times \int \frac{d^3 l}{(2\pi)^3} \frac{1}{(\Delta_b - \Delta_\alpha)\left[\frac{1}{2}(\Delta_b + \Delta_\alpha) + M_N\right] + \vec{p}^2 - \vec{l}^2}$$
$$= i\frac{G_F m_\pi^2}{16\pi M_N}\left(C^\alpha_{S(s)} + C^\alpha_{T(s)} \vec{\sigma}_1 \cdot \vec{\sigma}_2\right)\left(C^\alpha_{S(w)} + C^\alpha_{T(w)} \vec{\sigma}_1 \cdot \vec{\sigma}_2\right) \times \sqrt{(\Delta_b - \Delta_\alpha)\left[\frac{1}{2}(\Delta_b + \Delta_\alpha) + M_N\right] + \vec{p}^2}.$$

APPENDIX B: BALL DIAGRAMS

In our calculation we have two different kind of ball diagrams depending on the position of the weak vertex, although only one of them actually contributes. Their contribution can be written in terms of the B integrals defined in Appendix E.

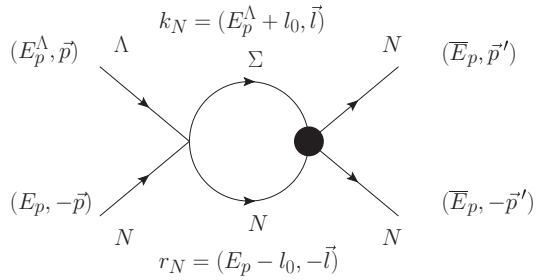

FIG. 14. Third caramel-type Feynman diagram.

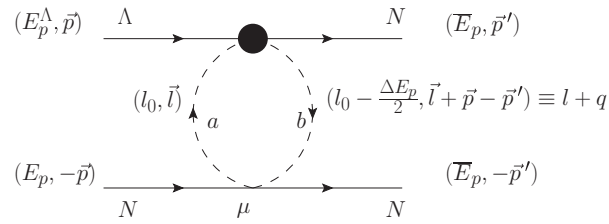

FIG. 15. Kinematical variables of the first kind of ball diagram.

Here and in the following sections we first write the relativistic amplitude using $V = i\ M$ and then the corresponding heavy-baryon expression.

For the first type of ball diagram, depicted in Fig. 15, we obtain the contribution

$$V_{\text{ball 1}} = \frac{G_F m_\pi^2 h_{2\pi}}{4 f_\pi^4}\delta_{ab}\,\epsilon^{abc}\tau^c \times \int \frac{d^4 l}{(2\pi)^4}\frac{1}{l^2 - m_\pi^2 + i\epsilon}\frac{1}{(l-q)^2 - m_\pi^2 + i\epsilon} \times \bar{u}_1(\overline{E}, \vec{p}\,')u_1\left(E_p^\Lambda, \vec{p}\right) \times \bar{u}_2(\overline{E}_p, -\vec{p}\,')\gamma_\mu(q^\mu - 2l^\mu)u_2(E_p, -\vec{p}) = 0,$$

which is shown to vanish owing to the isospin factor, $\delta_{ab}\epsilon^{abc}\tau^c = 0$.

The amplitude corresponding to the diagram in Fig. 16 reads

$$V_a = -i\frac{G_F m_\pi^2 h_{\Lambda N}}{8 f_\pi^4}(\vec{\tau}_1 \cdot \vec{\tau}_2) \times \int \frac{d^4 l}{(2\pi)^4}\frac{1}{l^2 - m_\pi^2 + i\epsilon}\frac{1}{(l+q)^2 - m_\pi^2 + i\epsilon} \times \frac{(2l^\mu + q^\mu)(q^\nu + 2l^\nu)}{k_N^2 - M_N^2 + i\epsilon} \times \bar{u}_1(\overline{E}, \vec{p}\,')\gamma_\mu(\not{k}_N + M_N)u_1\left(E_p^\Lambda, \vec{p}\right) \times \bar{u}_2(\overline{E}_p, -\vec{p}\,')\gamma_\nu u_2(E_p, -\vec{p}). \quad \text{(B1)}$$

Using heavy-baryon expansion,

$$V_a = \frac{G_F m_\pi^2 h_{\Lambda N}}{8\Delta M f_\pi^4}(\vec{\tau}_1 \cdot \vec{\tau}_2)\left(4B_{20} + 4q_0 B_{10} + q_0^2 B\right), \quad \text{(B2)}$$

where we have used the master integrals with $q_0 = -\frac{M_\Lambda - M_N}{2}$ and $\vec{q} = \vec{p}\,' - \vec{p}$.

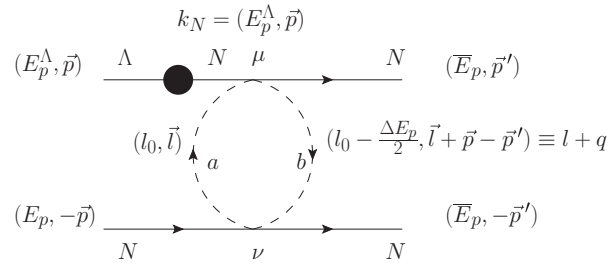

FIG. 16. Kinematical variables of the second kind of ball diagram.

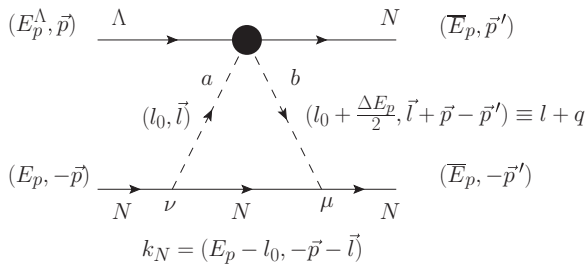

FIG. 17. Up triangle diagram contributing at NLO.

APPENDIX C: TRIANGLE DIAGRAMS

Two up triangles and two down triangles contribute to the interaction. The final expressions are written in terms of the integrals I defined in Appendix E . The amplitude for the first up triangle, depicted in Fig. 17, is

$$\begin{aligned} V_b = &-i\frac{3}{8}\frac{G_F m_\pi^2 h_{2\pi} g_A^2}{M_N f_\pi^4}\int\frac{d^4l}{(2\pi)^4}\frac{1}{l^2-m_\pi^2+i\epsilon}\\ &\times\frac{1}{(l+q)^2-m_\pi^2+i\epsilon}\frac{(l^\mu+q^\mu)l^\nu}{k_N^2-M_N^2+i\epsilon}\\ &\times\overline{u}_1(\overline{E}_p,\vec{p}\,')\overline{u}_1\big(E_p^\Lambda,\vec{p}\big)\\ &\times\overline{u}_2(\overline{E}_p,-\vec{p}\,')\gamma_\mu\gamma_5(\not{k}_N+M_N)\gamma_\nu\gamma_5 u_2(E_p,-\vec{p}). \end{aligned} \tag{C1}$$

Using heavy-baryon expansion,

$$V_b=\frac{3}{4}\frac{G_F m_\pi^2 h_{2\pi} g_A^2}{f_\pi^4}[(3-\eta)I_{22}+\vec{q}^{\,2}I_{23}+\vec{q}^{\,2}I_{11}], \tag{C2}$$

where, we have used the master integrals with $q_0=\frac{M_\Lambda-M_N}{2}$, $q_0'=0$, and $\vec{q}=\vec{p}\,'-\vec{p}$.

For the second up triangle, depicted in Fig. 18, the relativistic amplitude is

$$\begin{aligned} V_c = &-i\frac{G_F m_\pi^2 h_{\Lambda N} g_A^2}{8 f_\pi^4\big(r_N^2-M_N^2\big)}\vec{\tau}_1\cdot\vec{\tau}_2\int\frac{d^4l}{(2\pi)^4}\frac{1}{l^2-m_\pi^2+i\epsilon}\\ &\times\frac{1}{(l+q)^2-m_\pi^2+i\epsilon}\frac{(2l^\rho+q^\rho)(l^\mu+q^\mu)l^\nu}{k_N^2-M_N^2+i\epsilon}\\ &\times\overline{u}_1(\overline{E},\vec{p}\,')\gamma_\rho(\not{k}_N'+M_N)u_1\big(E_p^\Lambda,\vec{p}\big)\\ &\times\overline{u}_2(\overline{E}_p,-\vec{p}\,')\gamma_\mu\gamma_5(\not{k}_N+M_N)\gamma_\nu\gamma_5 u_2(E_p,-\vec{p}). \end{aligned} \tag{C3}$$

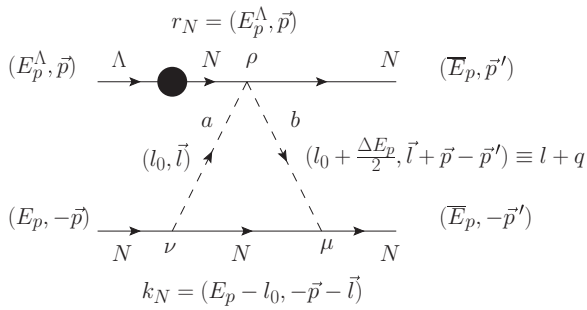

FIG. 18. Second up triangle contribution at NLO.

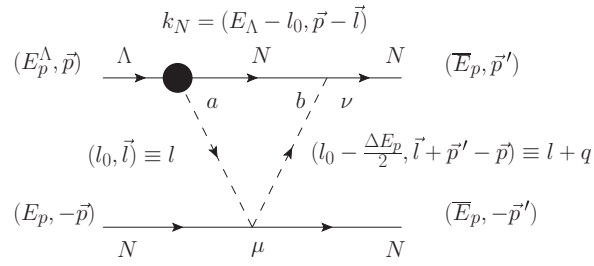

FIG. 19. Down triangle contribution at NLO.

Using heavy-baryon expansion,

$$\begin{aligned} V_c = &\frac{G_F m_\pi^2 h_{\Lambda N} g_A^2}{8\Delta M f_\pi^4}\vec{\tau}_1\cdot\vec{\tau}_2[2(3-\eta)I_{32}+2\vec{q}^{\,2}I_{33}+2\vec{q}^{\,2}I_{21}\\ &+(3-\eta)q_0 I_{22}+q_0\vec{q}^{\,2}I_{23}+q_0\vec{q}^{\,2}I_{11}], \end{aligned} \tag{C4}$$

where, we have used the master integrals with $q_0=\frac{M_\Lambda-M_N}{2}$, $q_0'=0$, and $\vec{q}=\vec{p}\,'-\vec{p}$.

The amplitude for the first down triangle (Fig. 19) is

$$\begin{aligned} V_d = &\,i\frac{G_F m_\pi^2 g_A}{4 f_\pi^3}(\vec{\tau}_1\cdot\vec{\tau}_2)\int\frac{d^4l}{(2\pi)^4}\frac{1}{l^2-m_\pi^2+i\epsilon}\\ &\times\frac{1}{(l+q)^2-m_\pi^2+i\epsilon}\frac{(l^\nu+q^\nu)(2l^\mu+q^\mu)}{k_N^2-M_N^2+i\epsilon}\\ &\times\overline{u}_1(\overline{E},\vec{p}\,')\gamma_\nu\gamma_5(\not{k}_N+M_N)(A+B\gamma_5)u_1\big(E_p^\Lambda,\vec{p}\big)\\ &\times\overline{u}_2(\overline{E}_p,-\vec{p}\,')\gamma_\mu u_2(E_p,-\vec{p}); \end{aligned} \tag{C5}$$

with the heavy-baryon expansion, it reduces to

$$\begin{aligned} V_d = &-\frac{G_F m_\pi^2 g_A}{8 M_N f_\pi^3}(\vec{\tau}_1\cdot\vec{\tau}_2)\big\{B\big[2I_{30}+7q_0 I_{20}+7q_0^2 I_{10}\\ &+2q_0^3 I-2(3-\eta)I_{32}-(3-\eta)q_0 I_{22}\big]\\ &-B(2I_{21}+q_0 I_{11}+2I_{33}+q_0 I_{23})\vec{q}^{\,2}\\ &-B(2I_{10}+2I_{21}+q_0 I+q_0 I_{11})(\vec{q}\cdot\vec{p})\\ &+2A\,M_N(2I_{21}+q_0 I_{11}-2I_{10}-q_0 I)\vec{\sigma}_1\cdot\vec{q}\\ &+iB(-2I_{21}-q_0 I_{11}+2I_{10}+q_0 I)\vec{\sigma}_1(\vec{q}\times\vec{p})\big\}. \end{aligned} \tag{C6}$$

We have used the master integrals with $q_0=-\frac{M_\Lambda-M_N}{2}$, $q_0'=-M_\Lambda+M_N$, and $\vec{q}=\vec{p}'-\vec{p}$.

The second type of down triangle diagram involves the intermediate exchange of the Σ (Fig. 20). Its

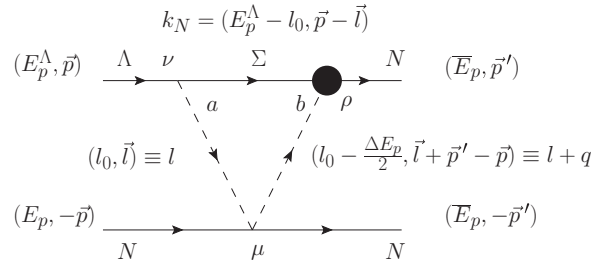

FIG. 20. Second type of down triangle involving the intermediate exchange of a Σ.

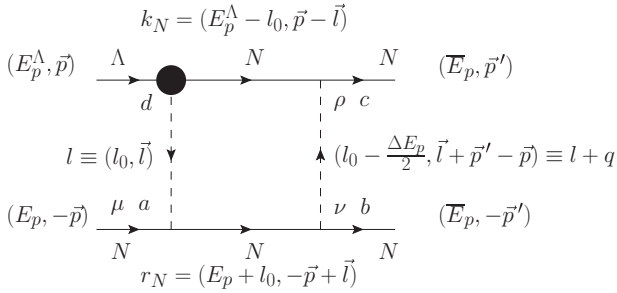

FIG. 21. Box diagram contributing at NLO.

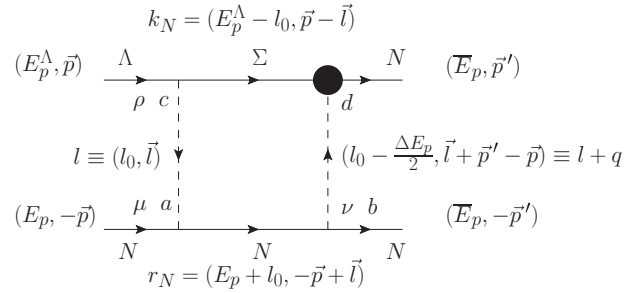

FIG. 22. Second box-type Feynman diagram.

amplitude is

$$V_e = \frac{G_F m_\pi^2 D_s}{4\sqrt{3} f_\pi^3} \int \frac{d^4 l}{(2\pi)^4} \frac{1}{l^2 - m_\pi^2 + i\epsilon} \times \frac{1}{(l+q)^2 - m_\pi^2 + i\epsilon} \frac{(2l^\mu + q^\mu) l^\nu}{k_N^2 - M_\Sigma^2 + i\epsilon} \times \bar{u}_1(\overline{E}, \vec{p}\,')(A_\Sigma + B_\Sigma \gamma_5)(\not{k}_N + M_\Sigma)\gamma_\nu \gamma_5 u_1\big(E_p^\Lambda, \vec{p}\big) \times \bar{u}_2(\overline{E}_p, -\vec{p}\,')\gamma_\mu u_2(E_p, -\vec{p}).$$

Using the heavy-baryon expansion

$$V_e = -\frac{G_F m_\pi^2 D_s}{8\sqrt{3} M_N f_\pi^3} \{B_\Sigma[-2I_{30} + (-5q_0 - 2\Delta M_\Sigma) I_{20} + 2(3-\eta) I_{32} + 2\vec{q}^2 I_{33} + 2\vec{q}^2 I_{21} + \vec{q}^2 I_{21} + q_0(-2q_0 - \Delta M_\Sigma) I_{10} + (3-\eta) q_0 I_{22} + q_0 \vec{q}^2 I_{23} + q_0 \vec{q}^2 I_{11}] - 2A_\Sigma M_N (2I_{21} + q_0 I_{11})(\vec{\sigma}_1 \cdot \vec{q})\}. \quad \text{(C7)}$$

The isospin is taken into account by replacing every A_Σ and B_Σ with

$$\tfrac{2}{3}(\sqrt{3} A_{\Sigma\frac{1}{2}} + A_{\Sigma\frac{3}{2}})\vec{\tau}_1 \cdot \vec{\tau}_2,\ \tfrac{2}{3}(\sqrt{3} B_{\Sigma\frac{1}{2}} + B_{\Sigma\frac{3}{2}})\vec{\tau}_1 \cdot \vec{\tau}_2,$$

where we have used the master integrals with $q_0 = -\frac{M_\Lambda - M_N}{2}$, $q_0' = M_\Sigma - M_\Lambda$, and $\vec{q} = \vec{p}\,' - \vec{p}$.

APPENDIX D: BOX DIAGRAMS

We have two kind of direct box diagrams and two cross-box ones. Direct box diagrams usually present a pinch singularity. This is because the poles appearing in the baryonic propagators get infinitesimally close to one another. In our integrals the denominators appearing in the baryonic propagators also contain terms proportional to $M_\Lambda - M_N$ and $M_\Sigma - M_\Lambda$, and this avoids the singularity.

The integrals entering in the expression of the amplitudes are the J and K defined in Appendix E . The amplitude for the first type of box diagram (Fig. 21) is

$$V_f = i\frac{G_F m_\pi^2 g_A^3}{8 f_\pi^3}(3 - 2\vec{\tau}_1 \cdot \vec{\tau}_2) \int \frac{d^4 l}{(2\pi)^4} \frac{1}{l^2 - m_\pi^2 + i\epsilon} \times \frac{1}{(l+q)^2 - m_\pi^2 + i\epsilon} \frac{1}{k_N^2 - M_N^2 + i\epsilon} a \times \frac{(l^\rho + q^\rho)(l^\nu + q^\nu) l^\mu}{r_N^2 - M_N^2 + i\epsilon} \times \bar{u}_1(\overline{E}, \vec{p}\,')\gamma_\rho \gamma_5 (\not{k}_N + M_N)(A + B\gamma_5) u_1\big(E_p^\Lambda, \vec{p}\big) \times \bar{u}_2(\overline{E}_p, -\vec{p}\,')\gamma_\nu \gamma_5 (\not{r}_N + M_N)\gamma_\mu \gamma_5 u_2(E_p, -\vec{p}).$$

Using the heavy-baryon expansion,

$$V_f = -\frac{G_F m_\pi^2 g_A^3}{32 M_N f_\pi^3}(3 - 2\vec{\tau}_1 \cdot \vec{\tau}_2)\big(- 4A M_N [4K_{22} + K_{11}\vec{q}^2 + 2K_{23}\vec{q}^2 + K_{35}\vec{q}^2 + (5-\eta)K_{34}]\vec{\sigma}_1 \cdot \vec{q} - 2B K_{22}(\vec{\sigma}_1 \cdot \vec{q})(\vec{\sigma}_2 \cdot \vec{q}) + 2B K_{22}(\vec{\sigma}_1 \cdot \vec{q})(\vec{\sigma}_2 \cdot \vec{p}) - 4iA M_N K_{22}(\vec{\sigma}_1 \times \vec{\sigma}_2) \cdot \vec{q} - 2B(\vec{p} \cdot \vec{q} - \vec{q}^2) K_{22} \vec{\sigma}_1 \cdot \vec{\sigma}_2 + 2iB[K_{11}\vec{q}^2 + 2K_{23}\vec{q}^2 + K_{35}\vec{q}^2(4-\eta)K_{22} + (5-\eta)K_{34}]\vec{\sigma}_1 \cdot (\vec{p} \times \vec{q}) + 2iB K_{22}\vec{\sigma}_2 \cdot (\vec{p} \times \vec{q}) - 2B\big\{K_{11}\vec{q}^2(\vec{p} \cdot \vec{q} + 2q_0^2) + K_{23}\big(2\vec{p} \cdot \vec{q}\vec{q}^2 + 2q_0^2\vec{q}^2 + \vec{q}^4\big) + K_{35}(\vec{p} \cdot \vec{q}\vec{q}^2 + 2\vec{q}^4) + K_{22}\big[(4-\eta)\vec{p} \cdot \vec{q} + \vec{q}^2 + (6-2\eta)q_0^2\big] + (5-\eta)K_{34}(\vec{p} \cdot \vec{q} + 2\vec{q}^2) + K_{48}\vec{q}^4 + K_{21}\vec{q}^2 q_0 + K_{33}\vec{q}^2 q_0 - K_{31}\vec{q}^2 - K_{43}\vec{q}^2 + 2(5-\eta)K_{47}\vec{q}^2 + (3-\eta)K_{32}q_0 - (3-\eta)K_{42} + (15 - 8\eta)K_{46}\big\}\big),$$

where we have used the master integrals with $q_0 = -\frac{M_\Lambda - M_N}{2}$, $q_0' = M_N - M_\Lambda$, and $\vec{q} = \vec{p}\,' - \vec{p}$.

The second box diagram (Fig. 22), which involves a Σ propagator, contributes with

$$V_g = -i\frac{G_F m_\pi^2 g_A^2 D_s}{4\sqrt{3} f_\pi^3} \int \frac{d^4 l}{(2\pi)^4} \frac{1}{l^2 - m_\pi^2 + i\epsilon} \times \frac{1}{(l+q)^2 - m_\pi^2 + i\epsilon} \frac{1}{k_N^2 - M_\Sigma^2 + i\epsilon} \times \frac{l^\rho (l^\nu + q^\nu) l^\mu}{r_N^2 - M_N^2 + i\epsilon} \times \bar{u}_1(\overline{E}, \vec{p}\,')(A_\Sigma + B_\Sigma \gamma_5)(\not{k}_N + M_N)\gamma_\rho \gamma_5 u_1\big(E_p^\Lambda, \vec{p}\big) \times \bar{u}_2(\overline{E}_p, -\vec{p}\,')\gamma_\nu \gamma_5 (\not{r}_N + M_N)\gamma_\mu \gamma_5 u_2(E_p, -\vec{p}). \quad \text{(D1)}$$

Using the heavy-baryon expansion,

$$V_g = \frac{G_F m_\pi^2 g_A^2 D_s}{16\sqrt{3} M_N f_\pi^3}\{-2B_\Sigma K_{22}\vec{q}^2 \vec{\sigma}_1 \cdot \vec{\sigma}_2 - 4A_\Sigma K_{22} M_N i(\vec{\sigma}_1 \times \vec{\sigma}_2)\vec{q} - 4A_\Sigma M_N(\vec{q}^2 K_{23} + 5K_{34} + \vec{q}^2 K_{35} + K_{22})\vec{\sigma}_1 \cdot \vec{q} + 2B_\Sigma K_{22}(\vec{\sigma}_1 \cdot \vec{q})(\vec{\sigma}_2 \cdot \vec{q}) + 2B_\Sigma[\vec{q}^2 K_{22} + \vec{q}^4 K_{23}$$

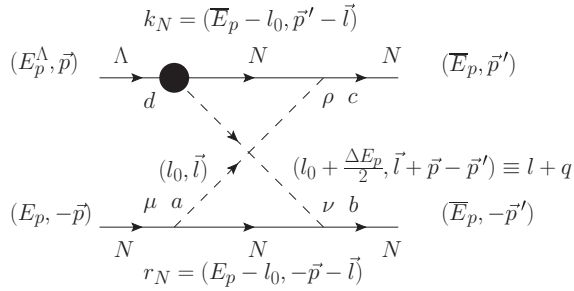

FIG. 23. Crossed-box diagram contributing at NLO.

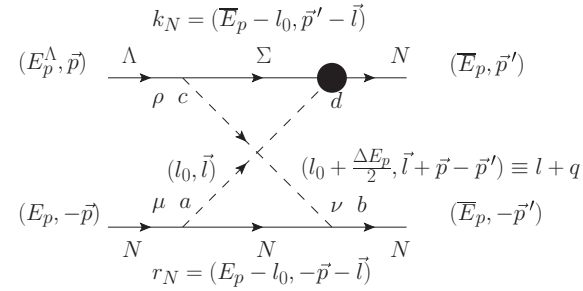

FIG. 24. Second crossed-box-type Feynman diagram.

$$
\begin{aligned}
&-\vec{q}^2 K_{31} + (3-\eta)(\Delta M - \Delta M_\Sigma) K_{32} \\
&+\vec{q}^2(\Delta M - \Delta M_\Sigma) K_{33} + 2(5-\eta)\vec{q}^2 K_{34} + 2\vec{q}^4 K_{35} \\
&-(3-\eta) K_{42} - \vec{q}^2 K_{43} + (15 - 8\eta) K_{46} \\
&+2(5-\eta)\vec{q}^2 K_{47} + \vec{q}^4 K_{48} + \vec{q}^2 K_{21}(\Delta \mathrm{M} - \Delta \mathrm{M}_\Sigma)]\}.
\end{aligned}
$$

To take into account the isospin we must replace every A_Σ and B_Σ with

$$
\begin{aligned}
A &\to -\sqrt{3} A_{\Sigma\frac{1}{2}} + 2A_{\Sigma\frac{3}{2}} + \tfrac{2}{3}\big(\sqrt{3}A_{\Sigma\frac{1}{2}} + A_{\Sigma\frac{3}{2}}\big)\vec{\tau}_1 \cdot \vec{\tau}_2, \\
B &\to -\sqrt{3} B_{\Sigma\frac{1}{2}} + 2B_{\Sigma\frac{3}{2}} + \tfrac{2}{3}\big(\sqrt{3}B_{\Sigma\frac{1}{2}} + B_{\Sigma\frac{3}{2}}\big)\vec{\tau}_1 \cdot \vec{\tau}_2.
\end{aligned}
$$

We have used the master integrals with $q_0 = -\frac{M_\Lambda - M_N}{2}$, $q_0' = M_\Sigma - M_\Lambda$, and $\vec{q} = \vec{p}\,' - \vec{p}$.

The first crossed-box diagram (Fig. 23) and contributes to the potential with

$$
\begin{aligned}
V_h = i\frac{G_F m_\pi^2 g_A^3}{8 f_\pi^3}(3 + 2\vec{\tau}_1 \cdot \vec{\tau}_2) \int \frac{d^4 l}{(2\pi)^4} \frac{1}{(l+q)^2 - m_\pi^2 + i\epsilon} \\
\times \frac{1}{l^2 - m_\pi^2 + i\epsilon} \frac{1}{r_N^2 - M_N^2 + i\epsilon} \frac{(l^\rho)(l^\nu + q^\nu)(l^\mu)}{k_N^2 - M_N^2 + i\epsilon} \\
\times \bar{u}_1(\overline{E}, \vec{p}\,')\gamma_\rho\gamma_5(\not{k}_N + M_N)(A + B\gamma_5)u_1\big(E_p^\Lambda, \vec{p}\big) \\
\times \bar{u}_2(\overline{E}_p, -\vec{p}\,')\gamma_\nu\gamma_5(\not{r}_N + M_N)\gamma_\mu\gamma_5 u_2(E_p, -\vec{p}).
\end{aligned}
$$

Using heavy-baryon expansion and the master integrals of Sec. VI, and redefining $\vec{q} \equiv \vec{p}\,' - \vec{p}$,

$$
\begin{aligned}
V_h = -\frac{G_F m_\pi^2 g_A^3}{32 M_N f_\pi^3}(3 + 2\vec{\tau}_1 \cdot \vec{\tau}_2)\{&-2iBJ_{22}\vec{\sigma}_2(\vec{p} \times \vec{q}) \\
&+2BJ_{22}(-\vec{p}\cdot\vec{q} + \vec{q}^2)\vec{\sigma}_1 \cdot \vec{\sigma}_2 \\
&+2iB[J_{22} + \vec{q}^2 J_{23} + (5+\eta)J_{34} + \vec{q}^2 J_{35}]\vec{\sigma}_1 \cdot (\vec{p} \times \vec{q}) \\
&+4iAJ_{22}M_N(\vec{\sigma}_1 \times \vec{\sigma}_2)\vec{q} + 4AM_N(\vec{q}^2 J_{23} + 5J_{34} \\
&+\vec{q}^2 J_{35} + J_{22})\vec{\sigma}_1 \cdot \vec{q} + 2BJ_{22}(\vec{\sigma}_1 \cdot \vec{q})(\vec{\sigma}_2 \cdot \vec{p}) \\
&-2BJ_{22}(\vec{\sigma}_1 \cdot \vec{q})(\vec{\sigma}_2 \cdot \vec{q}) - 2B[\vec{q}^2 q_0 J_{21} \\
&+(-\vec{p}\cdot\vec{q} + \vec{q}^2)J_{22} + (-\vec{p}\cdot\vec{q}\vec{q}^2 + \vec{q}^4)J_{23} \\
&-\vec{q}^2 J_{31} + (3-\eta)q_0 J_{32} + \vec{q}^2 q_0 J_{33} \\
&+(5-\eta)(-\vec{p}\cdot\vec{q} + 2\vec{q}^2)J_{34} + (-\vec{p}\cdot\vec{q}\vec{q}^2 + 2\vec{q}^4)J_{35} \\
&-(3-\eta)J_{42} - \vec{q}^2 J_{43} + (15-8\eta)J_{46} + 2(5-\eta)\vec{q}^2 J_{47} \\
&+\vec{q}^4 J_{48}]\}. \qquad \text{(D2)}
\end{aligned}
$$

We have used the master integrals with $q_0 = \frac{M_\Lambda - M_N}{2}$, $q_0' = -\frac{M_\Lambda - M_N}{2}$, and $\vec{q} = \vec{p}\,' - \vec{p}$.

The amplitude for the crossed-box diagram with a Σ propagator (Fig. 24) is

$$
\begin{aligned}
V_i = -i\frac{G_F m_\pi^2 g_A^2 D_s}{16\sqrt{3} M_N^2 f_\pi^3} \int \frac{d^4 l}{(2\pi)^4} \frac{1}{(l+q)^2 - m_\pi^2 + i\epsilon} \\
\times \frac{1}{l^2 - m_\pi^2 + i\epsilon} \frac{1}{r_N^2 - M_N^2 + i\epsilon} \\
\times \frac{(l^\rho + \vec{q}^\rho)(l^\nu + q^\nu)(l^\mu)}{k_N^2 - M_\Sigma^2 + i\epsilon} \\
\times \bar{u}_1(\overline{E}, \vec{p}\,')(A_\Sigma + B_\Sigma\gamma_5)(\not{k}_N + M_\Sigma)\gamma_\rho\gamma_5 u_1\big(E_p^\Lambda, \vec{p}\big) \\
\times \bar{u}_2(\overline{E}_p, -\vec{p}\,')\gamma_\nu\gamma_5(\not{r}_N + M_N)\gamma_\mu\gamma_5 u_2(E_p, -\vec{p}). \qquad \text{(D3)}
\end{aligned}
$$

Using heavy-baryon expansion and the master integrals of Sec. VI, and redefining $\vec{q} \equiv \vec{p}\,' - \vec{p}$,

$$
\begin{aligned}
V_i = \frac{G_F m_\pi^2 g_A^2 D_s}{16\sqrt{3} M_N f_\pi^3}\{&2B_\Sigma J_{22}\vec{q}^2\vec{\sigma}_1 \cdot \vec{\sigma}_2 \\
&-2iA_\Sigma J_{22}M_N(\vec{\sigma}_1 \times \vec{\sigma}_2)\cdot\vec{q} - A_\Sigma M_N(\vec{q}^2 J_{11} + 2\vec{q}^2 J_{23} \\
&+5J_{34} + \vec{q}^2 J_{35} + 4J_{22})\vec{\sigma}_1 \cdot \vec{q} \\
&-2B_\Sigma J_{22}(\vec{\sigma}_1 \cdot \vec{q})(\vec{\sigma}_2 \cdot \vec{q}) \\
&+2B_\Sigma\big[(\vec{q}^2 - (3-\eta)q_0(q_0 + \Delta M_\Sigma)J_{22} \\
&+\big(\vec{q}^4 - \vec{q}^2 q_0^2 - \vec{q}^2 q_0 \Delta M_\Sigma\big)J_{23} - \vec{q}^2 J_{31} \\
&-(3-\eta)(2q_0 + \Delta M_\Sigma)J_{32} - (2\vec{q}^2 q_0 + \vec{q}^2 \Delta M_\Sigma)J_{33} \\
&+2(5-\eta)\vec{q}^2 J_{34} + 2\vec{q}^4 J_{35} - (3-\eta)J_{42} - \vec{q}^2 J_{43} \\
&+(15-8\eta)J_{46} + 2(5-\eta)\vec{q}^2 J_{47} + \vec{q}^4 J_{48} \\
&-\vec{q}^2 q_0 J_{11}(q_0 + \Delta \mathrm{M}_\Sigma) - \vec{q}^2 J_{21}(2q_0 + \Delta \mathrm{M}_\Sigma)\big]\}.
\end{aligned}
$$

To take into account the isospin we must replace every A_Σ and B_Σ with

$$
\begin{aligned}
A_\Sigma &\to -\sqrt{3} A_{\Sigma\frac{1}{2}} + 2A_{\Sigma\frac{3}{2}} - \tfrac{2}{3}\big(\sqrt{3}A_{\Sigma\frac{1}{2}} + 2A_{\Sigma\frac{3}{2}}\big)\vec{\tau}_1 \cdot \vec{\tau}_2, \\
B_\Sigma &\to -\sqrt{3} B_{\Sigma\frac{1}{2}} + 2B_{\Sigma\frac{3}{2}} - \tfrac{2}{3}\big(\sqrt{3}B_{\Sigma\frac{1}{2}} + 2B_{\Sigma\frac{3}{2}}\big)\vec{\tau}_1 \cdot \vec{\tau}_2.
\end{aligned}
$$

We have used the master integrals with $q_0 = \frac{M_\Lambda - M_N}{2}$, $q_0' = M_\Sigma - M_\Lambda + \frac{M_\Lambda - M_N}{2}$, and $\vec{q} = \vec{p}\,' - \vec{p}$.

APPENDIX E: MASTER INTEGRALS

1. Definitions

We need the following integrals to calculate the Feynman diagrams. The B's, I's, J's, and K's appear, respectively, in the ball, triangle, box, and crossed-box diagrams:

$$B_{;\mu;\mu\nu} \equiv \frac{1}{i}\int \frac{d^4l}{(2\pi)^4}\frac{1}{l^2-m^2+i\epsilon}\frac{(1;l_\mu;l_\mu l_\nu)}{(l+q)^2-m^2+i\epsilon},$$

$$I_{;\mu;\mu\nu;\mu\nu\rho} \equiv \frac{1}{i}\int \frac{d^4l}{(2\pi)^4}\frac{1}{l^2-m^2+i\epsilon}\frac{1}{(l+q)^2-m^2+i\epsilon} \times \frac{1}{-l_0-q_0'+i\epsilon}(1;l_\mu;l_\mu l_\nu;l_\mu l_\nu l_\rho),$$

$$J_{;\mu;\mu\nu;\mu\nu\rho} \equiv \frac{1}{i}\int \frac{d^4l}{(2\pi)^4}\frac{1}{l^2-m^2+i\epsilon}\frac{1}{(l+q)^2-m^2+i\epsilon} \times \frac{1}{-l_0-q_0'+i\epsilon}\frac{(1;l_\mu;l_\mu l_\nu;l_\mu l_\nu l_\rho)}{-l_0+i\epsilon},$$

$$K_{;\mu;\mu\nu;\mu\nu\rho} \equiv \frac{1}{i}\int \frac{d^4l}{(2\pi)^4}\frac{1}{l^2-m^2+i\epsilon}\frac{1}{(l+q)^2-m^2+i\epsilon} \times \frac{1}{-l_0-q_0'+i\epsilon}\frac{(1;l_\mu;l_\mu l_\nu;l_\mu l_\nu l_\rho)}{l_0+i\epsilon}.$$

The strategy is to calculate explicitly the integrals with no subindex (no integrated momenta in the numerators) and then relate the others to simpler integrals. To do so, we also need to explicitly calculate the following integrals:

$$A(m) \equiv \frac{1}{i}\int \frac{d^4l}{(2\pi)^4}\frac{1}{l^2-m^2+i\epsilon},$$

$$A_{;\mu;\mu\nu}(q,q') \equiv \frac{1}{i}\int \frac{d^4l}{(2\pi)^4}\frac{1}{(l+q)^2-m^2+i\epsilon} \times \frac{1}{-l_0-q_0'+i\epsilon}(1;l_\mu;l_\mu l_\nu),$$

$$C_{;\mu;\mu\nu;\mu\nu\rho}(q_0,q_0') \equiv \frac{1}{i}\int \frac{d^4l}{(2\pi)^4}\frac{1}{(l+q)^2-m^2+i\epsilon} \times \frac{1}{-l_0-q_0'+i\epsilon}\frac{(1;l_\mu;l_\mu l_\nu;l_\mu l_\nu l_\rho)}{-l_0+i\epsilon},$$

$$D_{;\mu;\mu\nu;\mu\nu\rho}(q_0,q_0') \equiv \frac{1}{i}\int \frac{d^4l}{(2\pi)^4}\frac{1}{(l+q)^2-m^2+i\epsilon} \times \frac{1}{-l_0-q_0'+i\epsilon}\frac{(1;l_\mu;l_\mu l_\nu;l_\mu l_\nu l_\rho)}{l_0+i\epsilon}.$$

The integrals can be divided depending on their subindexes being temporal or spatial. We show explicitly all the cases for the integrals J. The same definitions are used for all the other integrals. Therefore, to know any other integral one needs to replace in Eq. (E1) J with A, B, I, etc.,

$$\begin{aligned}
J_\mu &\equiv \delta_{\mu0}J_{10} + \delta_{\mu i}J_{11}\vec{q}_i,\\
J_{\mu\nu} &\equiv \delta_{\mu0}\delta_{\nu0}J_{20} + (\delta_{\mu0}\delta_{\nu i}+\delta_{\mu i}\delta_{\nu0})J_{21}\vec{q}_i + \delta_{\mu i}\delta_{\nu j}(J_{22}\delta_{ij}+J_{23}\vec{q}_i\vec{q}_j),\\
J_{\mu\nu\rho} &\equiv \delta_{\mu0}\delta_{\nu0}\delta_{\rho0}J_{30} + \delta\delta\delta_{\{\mu\nu\rho00i\}}\vec{q}_i J_{31} + \delta\delta\delta_{\{\mu\nu\rho0ij\}}(\delta_{ij}J_{32}+\vec{q}_i\vec{q}_j J_{33}) + \delta_{\mu i}\delta_{\nu j}\delta_{\rho k}(\delta\vec{q}_{\{ijk\}}J_{34}+\vec{q}_i\vec{q}_j\vec{q}_k J_{35}),\\
J_{\mu\nu\rho\sigma} &\equiv \delta_{\mu0}\delta_{\nu0}\delta_{\rho0}\delta_{\sigma0}J_{40} + \delta\delta\delta\delta_{\{\mu\nu\rho\sigma000i\}}\vec{q}_i J_{41} + \delta\delta\delta\delta_{\{\mu\nu\rho\sigma00ij\}}(\delta_{ij}J_{42}+\vec{q}_i\vec{q}_j J_{43}) + \delta\delta\delta\delta_{\{\mu\nu\rho\sigma0ijk\}}(\delta\vec{q}_{\{ijk\}}J_{44}+\vec{q}_i\vec{q}_j\vec{q}_k J_{45}) + \delta_{\mu i}\delta_{\nu j}\delta_{\rho k}\delta_{\sigma l}(\delta\delta_{\{ijkl\}}J_{46}+\delta\vec{q}\vec{q}_{\{ijkl\}}J_{47} + \vec{q}_i\vec{q}_j\vec{q}_k\vec{q}_l J_{48}).
\end{aligned} \tag{E1}$$

All coefficients J_{10}, J_{11}, etc., have been written explicitly as functions of I, J, K, which can be integrated numerically, and the other simpler functions. The following definitions have been employed:

$$\begin{aligned}
\delta\vec{q}_{\{ijk\}} &= \delta_{ij}\vec{q}_k + \delta_{ik}\vec{q}_j + \delta_{jk}\vec{q}_i,\\
\delta\vec{q}\vec{q}_{\{ijkl\}} &= \delta_{ij}\vec{q}_k\vec{q}_l + \delta_{ik}\vec{q}_j\vec{q}_l + \delta_{il}\vec{q}_j\vec{q}_k + \delta_{jk}\vec{q}_i\vec{q}_l + \delta_{jl}\vec{q}_i\vec{q}_k + \delta_{kl}\vec{q}_i\vec{q}_j,\\
\delta\delta_{\{ijkl\}} &= \delta_{ij}\delta_{kl} + \delta_{ik}\delta_{jl} + \delta_{il}\delta_{jk}.
\end{aligned}$$

The other quantities, $\delta\delta\delta_{\{\mu\nu\rho00i\}}$, $\delta\delta\delta_{\{\mu\nu\rho0ij\}}$, etc., are not meant to be contracted with the indexes i, j, and k appearing in the rest of the expressions. They only indicate how many of the indexes μ, ν, ρ, and σ must be temporal and how many spatial. It does not matter the order in which 0, i, j, and k are assigned to μ, ν, ρ, and σ, because all the integrals $J_{\mu\nu}$, $J_{\mu\nu\rho}$, etc., are symmetric with respect to these indexes. For example,

$$J_{00i} = J_{0i0} = J_{i00} = \vec{q}_i J_{31}.$$

2. Results for the master integrals

We have regularized the master integrals via dimensional regularization, where the integrals depend on the momentum dimension D_η, or more specifically, on the parameter η, defined through $D_\eta = 4-\eta$, and on the renormalization scale μ, for which we have taken $\mu = m_\pi$. In the following we use

$$R = -\frac{2}{\eta} - 1 + \gamma - \ln(4\pi), \quad q_0'' = q_0' - q_0.$$

The integrals $A(m)$, $A(q_0,q_0')$, and $B(q_0,|\vec{q}|)$ appear, for example, in Ref. [26]. We have checked that both results coincide. It is important to maintain the $-i\epsilon$ prescription; otherwise the integrals may give a wrong result. We take it into account by replacing $q_0' \to q_0' - i\epsilon$ when evaluating the integrals.

a. $A(m)$, $A(q_0,q_0')$, and $B(q_0,\vec{q})$

We have

$$A(m) = -\frac{1}{8\pi^2}m^2\left[\frac{1}{2}R + \ln\left(\frac{m}{\mu}\right)\right], \tag{E2}$$

$$A(q_0,q_0') \equiv -\frac{q_0''}{8\pi^2}\left[\pi\frac{\sqrt{m^2-q_0''^2}}{q_0''} + 1 - R - 2\ln\left(\frac{m}{\mu}\right) - \frac{2\sqrt{(m^2-q_0''^2)}\arctan\left(\frac{q_0''}{\sqrt{m^2-q_0''^2}}\right)}{q_0''}\right], \tag{E3}$$

$$B(q_0,\vec{q}) = -\frac{1}{16\pi^2}\left[-1+R+2\ln\left(\frac{m}{\mu}\right)+2L(|q|)\right], \tag{E4}$$

with

$$L(|q|) \equiv \frac{w}{|q|}\ln\left(\frac{w+|q|}{2m}\right),$$

$w \equiv \sqrt{4m^2+|q|^2}$, $|q| \equiv \sqrt{\vec{q}^2-q_0^2}$, and $q^2 \equiv q_0^2-\vec{q}^2 \leqslant 0$.

b. $C(q_0, q_0')$ and $D(q_0, q_0')$

We have

$$C(q_0,q_0') = \frac{1}{8\pi^2 q_0'}\Bigg[\pi(v-v'') + q_0'(-1+R) + 2v\ \arctan\left(\frac{q_0}{v}\right) - 2v''\ \arctan\left(\frac{q_0''}{v''}\right)\Bigg],$$

with $v \equiv \sqrt{m^2-q_0^2}$ and $v'' \equiv \sqrt{m^2-q_0''^2}$, and

$$D(q_0,q_0') = -C(q_0,q_0') + \tfrac{1}{q_0'}\tfrac{1}{4\pi}\sqrt{m^2-q_0^2}.$$

c. $I(q_0, |\vec{q}|, q_0')$

We have

$$I(q_0,q,q_0') = -\frac{1}{8\pi^2}\int_0^1 dx\int_0^1 dy\left[\frac{\pi}{2}\frac{1}{\sqrt{s_x}} - \frac{3}{4}y^{-\frac{1}{2}}(1-y)C_q'\frac{1}{s_{xy}} + \frac{1}{2}y^{\frac{1}{2}}(1-y)C_q'^3\frac{1}{s_{xy}^2}\right],$$

with $C_q' = -q_0(1-x)+q_0'$, $s_x \equiv -q^2x(1-x)-(q_0'-q_0+q_0x)^2+m_\pi^2$, and $s_{xy} \equiv -q^2x(1-x)-(q_0'-q_0+q_0x)^2(1-y)+m_\pi^2$.

d. $J(q_0, |\vec{q}|, q_0')$ and $K(q_0, |\vec{q}|, q_0')$

We have

$$\begin{aligned}J = -\frac{1}{8\pi^2}\int_0^1 dx\int_0^1 dy\, y(1-y)\Bigg(&\big[-C_q'^3 - C_q'^2C_q - C_q'C_q^2 - C_q^3 + 2s_x(C_q'+C_q)\big]\frac{3\pi}{8s_{xy}^{\frac{5}{2}}}\\ &+(C_q'+C_q)\frac{\pi}{8s_{xy}^{\frac{3}{2}}} + \frac{105}{16}\int_0^1 dz\, z^3\sqrt{1-z}\Bigg\{-\frac{3}{s_{xyz}}\\ &+\big(C_q'^2 - 5C_q'C_q + C_q^2 - 9s_x\big)\frac{2}{7s_{xyz}^2}\\ &+\big[-9s_x^2 + 2s_x\big(C_q'^2 - 5C_q'C_q + C_q^2\big) + 3C_q'^3C_q + C_q'^2C_q^2 + 3C_q'C_q^3\big]\frac{8}{35s_{xyz}^3}\\ &+\big[-3s_x^3 + s_x^2\big(C_q'^2 - 5C_q'C_q + C_q^2\big) + s_x\big(3C_q'^3C_q + C_q'^2C_q^2 + 3C_q'C_q^3\big) - C_q'^3C_q^3\big]\frac{16}{35s_{xyz}^4}\Bigg\}\Bigg),\end{aligned}$$

with $C_q \equiv -q_0(1-x)$, $C_q' \equiv -q_0(1-x)+q_0'$, $s_x \equiv -q^2x(1-x)+m_\pi^2$, $s_{xy} \equiv s_x - C_q^2 + y(C_q^2 - C_q'^2)$, and $s_{xyz} \equiv s_x + z\cdot y(C_q^2 - C_q'^2) - zC_q^2$.

$$K = -J + \frac{1}{8\pi q_0'}\int_0^1 dx\frac{1}{\sqrt{m^2+(1-x)\big(\vec{q}^2x - q_0^2\big)}}.$$

3. Results for the master integrals with $q_0 = q_0' = 0$

We have

$$\begin{aligned}A(m) &= -\frac{1}{8\pi^2}m^2\left[\frac{1}{2}R + \ln\left(\frac{m}{\mu}\right)\right],\\ A(0,0) &= -\frac{m}{8\pi},\\ B(0,\vec{q}) &= -\frac{1}{16\pi^2}\left[-1+R+2\ln\left(\frac{m}{\mu}\right)+2L(q)\right],\\ C(0,0) &= -\frac{1}{4\pi^2}\left[-\frac{R}{2}-\frac{1}{2}-\ln\left(\frac{m}{\mu}\right)\right],\\ I(0,\vec{q},0) &= -\frac{1}{4\pi}At(q),\\ J(0,\vec{q},0) &= \frac{1}{2\pi^2\vec{q}^2}L(q),\end{aligned}$$

where $L(q)$ and $At(q)$ are defined with

$$\begin{aligned}At(q) &\equiv \frac{1}{2q}\arctan\left(\frac{q}{2m_\pi}\right),\\ L(q) &\equiv \frac{\sqrt{4m_\pi^2+q^2}}{q}\ln\left(\frac{\sqrt{4m_\pi^2+q^2}+q}{2m_\pi}\right).\end{aligned}$$

4. Relations between master integrals

a. $A_\mu(q_0, q_0')$

We have

$$A_{10} = -A(m) - q_0'A, \quad A_{11} = -A.$$

b. $A_{\mu\nu}(q, q')$

We have

$$A_{20} = \big[(q_0+q_0')A(m) + q_0'^2A\big], \quad A_{21} = A(m) + q_0'A,$$
$$A_{22} = \frac{1}{D_\eta - 1}\big[q_0''A(m) + (q_0''^2 - m^2)A\big], \quad A_{23} = A.$$

c. $B_\mu(q)$

We have

$$B_{10} = -\frac{q_0}{2}B, \quad B_{11} = -\frac{1}{2}B.$$

d. $B_{\mu\nu}(q)$

We have

$$B_{20} = \frac{1}{2(D_\eta-1)q^2}\left\{\left[q^2+q_0^2(D_\eta-2)\right]A(m) - \left[2\vec{q}^2m^2+\frac{1}{2}q^2(q^2-D_\eta q_0^2)\right]B\right\},$$
$$B_{21} = \frac{q_0}{2(D_\eta-1)q^2}\left[(D_\eta-2)A(m)+\left(\frac{D_\eta}{2}q^2-2m^2\right)B\right],$$
$$B_{22} = -\frac{1}{2(D_\eta-1)}\left[A(m)+\left(2m^2-\frac{q^2}{2}\right)B\right],$$
$$B_{23} = \frac{1}{2(D_\eta-1)q^2}\left[(D_\eta-2)A(m)+\left(\frac{D_\eta}{2}q^2-2m^2\right)B\right].$$

e. $C_\mu(q_0, q_0')$

We have

$$C_{10} = -A, \quad C_{11} = -C.$$

f. $C_{\mu\nu}(q_0, q_0')$

We have

$$C_{20} = -A_{10}, \quad C_{21} \equiv -A_{11},$$
$$C_{22} = \frac{1}{D_\eta-1}\left[C_{20}+2q_0C_{10}+\left(q_0^2-m^2\right)C\right], \quad C_{23} = C.$$

g. $C_{\mu\nu\rho}(q_0, q_0')$

We have

$$C_{30} = -A_{20}, \quad C_{31} = -A_{21},$$
$$C_{32} = -A_{22}, \quad C_{33} = -A_{23}$$
$$C_{34} \equiv -C_{22}, \quad C_{35} = -6C_{11}-3C_{23}-4C.$$

h. $D_\mu(q_0, q_0')$

We have

$$D_{10} = A, \quad D_{11} = -D.$$

i. $D_{\mu\nu}(q_0, q_0')$

We have

$$D_{20} \equiv A_{10}, \quad D_{21} \equiv A_{11},$$
$$D_{22} = \frac{1}{D_\eta-1}\left[D_{20}+2q_0D_{10}+\left(q_0^2-m^2\right)D\right], \quad D_{23} = D.$$

j. $D_{\mu\nu\rho}(q_0, q_0')$

We have

$$D_{30} \equiv A_{20}, \quad D_{31} \equiv A_{21},$$
$$D_{32} \equiv A_{20}, \quad D_{33} \equiv A_{21},$$
$$D_{34} \equiv -D_{22}, \quad D_{35} \equiv -6D_{11}-3D_{23}-4D.$$

k. I_μ

We have

$$I_{10} = -B-q_0'I,$$
$$I_{11} = \frac{1}{2\vec{q}^2}\left[-A(0,q_0',r_0)+A-2q_0B+\left(q_0^2-\vec{q}^2-2q_0q_0'\right)I\right].$$

l. $I_{\mu\nu}$

We have

$$I_{20} = -B_{10}-q_0'I_{10}, \quad I_{21} = -B_{11}-q_0'I_{11},$$
$$I_{22} = \frac{1}{(D_\eta-2)\vec{q}^{\,2}}[-I_{(\vec{l}\cdot\vec{q})^2}+\vec{q}^2I_{(\vec{l}^2)}],$$
$$I_{23} = \frac{1}{(D_\eta-2)\vec{q}^{\,4}}[(D_\eta-1)I_{(\vec{l}\cdot\vec{q})^2}-\vec{q}^2I_{(\vec{l}^2)}],$$
$$I_{(\vec{l}^2)} = -A(q,q')-m^2I_0-B_{10}-q_0'I_{10},$$
$$I_{(\vec{l}\cdot\vec{q})^2} = \frac{1}{2}\vec{q}^2[A_{11}(q,q')-2q_0B_{11}+(q^2-2q_0q_0')I_{11}].$$

m. $I_{\mu\nu\rho}$

We have

$$I_{30} = -B_{20}-q_0'I_{20}, \quad I_{31} = -B_{21}-q_0'I_{21},$$
$$I_{32} = -B_{22}-q_0'I_{22}, \quad I_{33} = -B_{23}-q_0'I_{23},$$
$$I_{34} = \frac{-I_{(\vec{l}\cdot\vec{q})^3}+\vec{q}^2I_{(\vec{l}\cdot\vec{q})\vec{l}^2}}{\vec{q}^4(D_\eta-2)}, \quad I_{35} = \frac{(D_\eta+1)I_{(\vec{l}\cdot\vec{q})^3}-3\vec{q}^2I_{(\vec{l}\cdot\vec{q})\vec{l}^2}}{\vec{q}^6(D_\eta-2)},$$
$$I_{(\vec{l}\cdot\vec{q})^3} = \tfrac{1}{2}\vec{q}^2[-A_{22}(0,q_0')-\vec{q}^2A_{23}(0,q_0')-\vec{q}^2A(0,q_0') - 2\vec{q}^2A_{11}(0,q_0')A_{22}+\vec{q}^2A_{23}+q^2I_{22}+q^2\vec{q}^2I_{23} - 2q_0B_{22}-2q_0\vec{q}^2B_{23}-2q_0q_0'I_{22}-2q_0q_0'\vec{q}^2I_{23}],$$
$$I_{(\vec{l}\cdot\vec{q})\vec{l}^2} = \vec{q}^2(-A_{11}-m^2I_{11}-B_{21}-q_0'I_{21}).$$

n. J_μ

We have

$$J_{10} \equiv -I, \quad J_{11} \equiv \frac{1}{2\vec{q}^2}[-C(0,q_0')+C-2q_0I+q^2J].$$

o. $J_{\mu\nu}$

We have

$$
\begin{aligned}
&J_{20} \equiv -I_{10}, \quad J_{21} \equiv -I_{11},\\
&J_{22} \equiv \frac{1}{(D_\eta-2)\vec{q}^{\,2}}[-J_{(\vec{l}\cdot\vec{q})^2} + \vec{q}^{\,2} J_{(\vec{l}^2)}],\\
&J_{23} \equiv \frac{1}{(D_\eta-2)\vec{q}^{\,4}}[(D_\eta-1)J_{(\vec{l}\cdot\vec{q})^2} - \vec{q}^{\,2} J_{(\vec{l}^2)}],\\
&J_{(\vec{l}^2)} = -C - m^2 J - I_{10},\\
&J_{(\vec{l}\cdot\vec{q})^2} = \tfrac{1}{2}[C_{11} + q^2 J_{11} - 2q_0 I_{11}]\vec{q}^{\,2}.
\end{aligned}
$$

p. $J_{\mu\nu\rho}$

We have

$$
\begin{aligned}
&J_{30} \equiv -I_{20}, \quad J_{31} \equiv -I_{21},\\
&J_{32} \equiv -I_{22}, \quad J_{33} \equiv -I_{23},\\
&J_{34} \equiv \frac{-J_{(\vec{l}\cdot\vec{q})^3} + \vec{q}^{\,2} J_{(\vec{l}\cdot\vec{q})\vec{l}^2}}{\vec{q}^4(D_\eta-2)},\\
&J_{35} \equiv \frac{(D_\eta+1)J_{(\vec{l}\cdot\vec{q})^3} - 3\vec{q}^{\,2} J_{(\vec{l}\cdot\vec{q})\vec{l}^2}}{\vec{q}^6(D_\eta-2)},\\
&J_{(\vec{l}\cdot\vec{q})^3} = \frac{\vec{q}^{\,2}}{2}[-C_{20}(0,q_0') - \vec{q}^{\,2}C_{21}(0,q_0') - \vec{q}^{\,2}C(0,q_0')\\
&\quad - 2\vec{q}^{\,2}C_{11}(0,q_0') + C_{20} + C_{21}\vec{q}^{\,2}\\
&\quad + q^2(J_{22} + J_{23}\vec{q}^{\,2}) - 2q_0(I_{22} + I_{23}\vec{q}^{\,2})],\\
&J_{(\vec{l}\cdot\vec{q})\vec{l}^2} = -\vec{q}^{\,2}[C_{11} + m^2 J_{11} + I_{21}].
\end{aligned}
$$

q. $J_{\mu\nu\rho\sigma}$

We have

$$
\begin{aligned}
&J_{40} \equiv -I_{30}, \quad J_{41} \equiv -I_{31},\\
&J_{42} \equiv -I_{32}, \quad J_{43} \equiv -I_{33},\\
&J_{44} \equiv -I_{34}, \quad J_{45} \equiv -I_{35},\\
&J_{46} = 2\frac{-J_{\vec{l}^2(\vec{l}\cdot\vec{q})^2} + \vec{q}^{\,2} J_{\vec{l}^4}}{\vec{q}^2(D-2)(2D+3)},\\
&J_{47} = \frac{-(2D+3)J_{(\vec{l}\cdot\vec{q})^4} + 2(2+D)\vec{q}^{\,2} J_{\vec{l}^2(\vec{l}\cdot\vec{q})^2} - \vec{q}^{\,4} J_{\vec{l}^4}}{\vec{q}^6(D-2)(2D+3)},\\
&J_{48} = \frac{(D+4)J_{(\vec{l}\cdot\vec{q})^4} - 6\vec{q}^{\,2} J_{\vec{l}^2(\vec{l}\cdot\vec{q})^2}}{\vec{q}^8(D-2)},\\
&J_{(\vec{l}\cdot\vec{q})^4} = \frac{\vec{q}^{\,4}}{2}[3C_{34} + \vec{q}^{\,2}C_{35} + q^2(3J_{34} + \vec{q}^{\,2}J_{35})\\
&\quad - 2q_0(3I_{34} + \vec{q}^{\,2}I_{35})],\\
&J_{\vec{l}^2(\vec{l}\cdot\vec{q})^2} = -\vec{q}^{\,2}[C_{22} + \vec{q}^{\,2}C_{23} + m^2(J_{22} + J_{23}\vec{q}^{\,2}) + I_{32}\\
&\quad + \vec{q}^{\,2}I_{33}],\\
&J_{\vec{l}^4} = -[C_{22}(D_\eta-1) + C_{23}\vec{q}^{\,2}]\\
&\quad - m^2[J_{22}(D_\eta-1) + J_{23}\vec{q}^{\,2}] - [I_{32}(D_\eta-1)\\
&\quad + I_{33}\vec{q}^{\,2}].
\end{aligned}
$$

r. K_μ

We have

$$
K_{10} = I, \quad K_{11} \equiv \frac{1}{2\vec{q}^{\,2}}[-D(0,q_0') + D + q^2K + 2q_0 I].
$$

s. $K_{\mu\nu}$

For the first two cases we apply the tricks

$$
\begin{aligned}
&K_{20} \equiv I_{10}, \quad K_{21} \equiv I_{11},\\
&K_{22} \equiv \frac{1}{(D_\eta-2)\vec{q}^{\,2}}[-K_{(\vec{l}\cdot\vec{q})^2} + \vec{q}^{\,2}K_{(\vec{l}^2)}],\\
&K_{23} \equiv \frac{1}{(D_\eta-2)\vec{q}^{\,4}}[(D_\eta-1)K_{(\vec{l}\cdot\vec{q})^2} - \vec{q}^{\,2}K_{(\vec{l}^2)}],
\end{aligned}
$$

giving the following results

$$
\begin{aligned}
&K_{(\vec{l}^2)} = -D - m^2K + I_{10} - r_0K_{10},\\
&K_{(\vec{l}\cdot\vec{q})^2} = \tfrac{1}{2}[D_{11} + q^2K_{11} + 2q_0I_{11}]\vec{q}^{\,2}.
\end{aligned}
$$

t. $K_{\mu\nu\rho}$

We have

$$
\begin{aligned}
&K_{30} \equiv I_{20}, \quad K_{31} \equiv I_{21},\\
&K_{32} \equiv I_{22}, \quad K_{33} \equiv I_{23},\\
&K_{34} = \frac{-K_{(\vec{l}\cdot\vec{q})^3} + \vec{q}^{\,2}K_{(\vec{l}\cdot\vec{q})\vec{l}^2}}{\vec{q}^4(D_\eta-2)},\\
&K_{35} \equiv \frac{(D_\eta+1)K_{(\vec{l}\cdot\vec{q})^3} - 3\vec{q}^{\,2}K_{(\vec{l}\cdot\vec{q})\vec{l}^2}}{\vec{q}^6(D_\eta-2)},\\
&K_{(\vec{l}\cdot\vec{q})^3} = \frac{\vec{q}^{\,2}}{2}[-D_{22}(0,q_0') - \vec{q}^{\,2}D_{23}(0,q_0') - \vec{q}^{\,2}D(0,q_0')\\
&\quad - 2\vec{q}^{\,2}D_{11}(0,q_0') + D_{22} + \vec{q}^{\,2}D_{23}\\
&\quad + q^2(K_{22} + K_{23}\vec{q}^{\,2}) + 2q_0(I_{22} + I_{23}\vec{q}^{\,2})],\\
&K_{(\vec{l}\cdot\vec{q})\vec{l}^2} = -\vec{q}^{\,2}[D_{11} + m^2K_{11} - I_{21} + r_0K_{21}].
\end{aligned}
$$

u. $K_{\mu\nu\rho\sigma}$

We have

$$
\begin{aligned}
&K_{40} \equiv I_{30}, \quad K_{41} \equiv I_{31},\\
&K_{42} \equiv I_{32}, \quad K_{43} \equiv I_{33},\\
&K_{44} \equiv I_{34}, \quad K_{45} \equiv I_{35},\\
&K_{46} = 2\,\frac{-K_{\vec{l}^2(\vec{l}\cdot\vec{q})^2} + \vec{q}^{\,2}K_{\vec{l}^4}}{\vec{q}^2(D-2)(2D+3)},\\
&K_{47} = \frac{-(2D+3)K_{(\vec{l}\cdot\vec{q})^4} + 2(2+D)\vec{q}^{\,2}K_{\vec{l}^2(\vec{l}\cdot\vec{q})^2} - \vec{q}^{\,4}K_{\vec{l}^4}}{\vec{q}^6(D-2)(2D+3)},\\
&K_{48} = \frac{(D+4)K_{(\vec{l}\cdot\vec{q})^4} - 6\vec{q}^{\,2}K_{\vec{l}^2(\vec{l}\cdot\vec{q})^2}}{\vec{q}^8(D-2)},
\end{aligned}
$$

$$K_{(\vec{l}\cdot\vec{q})^4} = \tfrac{1}{2}[2D_{10}\vec{q}^4 + \vec{q}^4 D + q^2(K_{22}\vec{q}^2 + K_{23}\vec{q}^4) + 2q_0(I_{22}\vec{q}^2 + I_{23}\vec{q}^4)],$$
$$K_{\vec{l}^2(\vec{l}\cdot\vec{q})^2} = -[D_{22} + D_{23}\vec{q}^2 + m^2(K_{22} + K_{23}\vec{q}^2) - I_{32} - I_{33}\vec{q}^2]\vec{q}^2,$$
$$K_{\vec{l}^4} = -[D_{22}(D_\eta - 1) + D_{23}\vec{q}^2] - m^2[K_{22}(D_\eta - 1) + K_{23}\vec{q}^2] + [I_{32}(D_\eta - 1) + I_{33}\vec{q}^2].$$

[1] D. R. Entem and R. Machleidt, Phys. Rev. C **68**, 041001(R) (2003); Phys. Rep. **503**, 1 (2011).
[2] E. Epelbaum, W. Glockle and U.-G. Meißner, Nucl. Phys. A **747**, 362 (2005); E. Epelbaum and U.-G. Meißner, Annu. Rev. Nucl. Part. Sci. **62**, 159 (2012).
[3] Shi-Lin Zhu, C. M. Maekawa, B. R. Holstein, M. J. Ramsey-Musolf, and U. van Kolck, Nucl. Phys. A **748**, 435 (2005).
[4] M. J. Savage and M. B. Wise, Phys. Rev. D **53**, 349 (1996).
[5] C. L. Korpa, A. E. L. Dieperink, and R. G. E. Timmermans, Phys. Rev. C **65**, 015208 (2001).
[6] H. W. Hammer, Nucl. Phys. A **705**, 173 (2002).
[7] S. R. Beane, P. F. Bedaque, A. Parreño, and M. J. Savage, Nucl. Phys. A **747**, 55 (2005).
[8] H. Polinder, J. Haidenbauer, and Ulf-G. Meißner, Nucl. Phys. A **779**, 244 (2006).
[9] Jung-Hwan Jun, Phys. Rev. C **63**, 044012 (2001).
[10] A. Parreño, C. Bennhold, and B. R. Holstein, Phys. Rev. C **70**, 051601 (2004); Nucl. Phys. A **754**, 127c (2005).
[11] A. Pérez-Obiol, A. Parreño, and B. Juliá-Díaz, Phys. Rev. C **84**, 024606 (2011).
[12] J. Haidenbauer, K. Holinde, K. Kilian, T. Sefzick, and A. W. Thomas, Phys. Rev. C **52**, 3496 (1995).
[13] A. Parreño, A. Ramos, N. G. Kelkar, and C. Bennhold, Phys. Rev. C **59**, 2122 (1999).
[14] T. Inoue, K. Sasaki, and M. Oka, Nucl. Phys. A **684**, 478 (2001).
[15] T. Kishimoto, A. Sakaguchi, S. Ajimura, Y. Shimizu, H. Kohri, S. Minami, T. Mori, M. Sumihama *et al.*, Nucl. Phys. A **663**, 509 (2000).
[16] S. Ajimura, H. Hayakawa, T. Itabashi, T. Kanie, T. Kishimoto, H. Kohri, K. Matsuoka, S. Minami *et al.*, Nucl. Phys. A **691**, 312 (2001).
[17] J. F. Dubach, G. B. Feldman, B. R. Holstein, and L. de la Torre, Ann. Phys. **249**, 146 (1996).
[18] J. F. Donohue, E. Golovich, and B. R. Holstein, *Dynamics of the Standard Model* (Cambridge University Press, Cambridge, 1992).
[19] B. Holzenkamp, K. Holinde, and J. Speth, Nucl. Phys. A **500**, 485 (1989).
[20] V. G. J. Stoks and Th. A. Rijken, Phys. Rev. C **59**, 3009 (1999); Th. A. Rijken, V. G. J. Stoks, and Y. Yamamoto, *ibid.* **59**, 21 (1999).
[21] S. Weinberg, Phys. Lett. B **251**, 288 (1990); Nucl. Phys. B **363**, 3 (1991).
[22] E. Jenkins and A. Manohar, Phys. Lett. B **255**, 558 (1991).
[23] A. Parreño, A. Ramos, and C. Bennhold, Phys. Rev. C **56**, 339 (1997).
[24] D. Jido, E. Oset, and J. E. Palomar, Nucl. Phys. A **694**, 525 (2001).
[25] E. Oset, H. Toki, M. Mizobe, and T. T. Takahashi, Prog. Theor. Phys. **103**, 351 (2000).
[26] S. Scherer, Adv. Nucl. Phys. **27**, 277 (2003).